Peng *et al. Chem Synth* 2023;3:47
DOI: 10.20517/cs.2023.34

Chemical Synthesis

Review

Open Access

Check for updates

Strain engineering of two-dimensional materials for energy storage and conversion applications

Xing Peng[#], Long Chen[#], Yifan Liu, Chao Liu, Honglan Huang, Jinbo Fan, Pan Xiong[*], Junwu Zhu[*]

Key Laboratory for Soft Chemistry and Functional Materials of Ministry Education, School of Chemistry and Chemical Engineering, Nanjing University of Science and Technology, Nanjing 210094, Jiangsu, China.
[#]Authors contributed equally.

[*]**Correspondence to:** Profs. Pan Xiong, Junwu Zhu, Key Laboratory for Soft Chemistry and Functional Materials of Ministry Education, School of Chemistry and Chemical Engineering, Nanjing University of Science and Technology, 200 Xiaolingwei Street, Xuanwu District, Nanjing 210094, Jiangsu, China. E-mail: pan.xiong@njust.edu.cn; zhujw@njust.edu.cn

How to cite this article: Peng X, Chen L, Liu Y, Liu C, Huang H, Fan J, Xiong P, Zhu J. Strain engineering of two-dimensional materials for energy storage and conversion applications. *Chem Synth* 2023;3:47. https://dx.doi.org/10.20517/cs.2023.34

Received: 4 Jul 2023 **First Decision:** 14 Sep 2023 **Revised:** 27 Sep 2023 **Accepted:** 24 Oct 2023 **Published:** 7 Dec 2023

Academic Editors: Aicheng Chen, Da-Gang Yu **Copy Editor:** Dong-Li Li **Production Editor:** Dong-Li Li

Abstract

Two-dimensional (2D) materials have garnered much interest due to their exceptional optical, electrical, and mechanical properties. Strain engineering, as a crucial approach to modulate the physicochemical characteristics of 2D materials, has been widely used in various fields, especially for energy storage and conversion. Herein, the recent progress in strain engineering of 2D materials is summarized for energy storage and conversion applications. The fundamental understanding of strain in 2D materials is first described. Then, some synthetic methods for modulating the properties of 2D materials via strain engineering are introduced. Further, the applications of strain engineering of 2D materials in energy storage, photocatalysis, and electrocatalysis are discussed. Finally, the challenges and perspectives on strain engineering of 2D materials are also outlined.

Keywords: Two-dimensional materials, strain engineering, energy storage and conversion, electrocatalysis, photocatalysis

INTRODUCTION

The awareness of two-dimensional (2D) materials has been steadily growing among the public since the discovery of graphene through mechanical exfoliation in 2004[1]. Thanks to the ultrathin characteristics of 2D materials, they exhibit favorable morphological, electrical, optical, magnetic, and chemical properties[2-6].

© The Author(s) 2023. **Open Access** This article is licensed under a Creative Commons Attribution 4.0 International License (https://creativecommons.org/licenses/by/4.0/), which permits unrestricted use, sharing, adaptation, distribution and reproduction in any medium or format, for any purpose, even commercially, as long as you give appropriate credit to the original author(s) and the source, provide a link to the Creative Commons license, and indicate if changes were made.

Compared with the bulk structure of three-dimensional (3D) materials, 2D materials exhibit remarkable properties in energy storage and catalysis due to their large specific surface and fully exposed atoms[7-11]. To broaden the utilization of 2D materials, diverse approaches have been developed to adjust their properties, such as doping[12,13], defects engineering[14,15], alloying[16], substrate engineering[17], and heterostructures[18], *etc*.

Among these methods, strain engineering is widely employed to modify the properties of 2D materials due to its simplicity and large adjustable range. The application of strain on the surface of 2D materials is intricately related to the electronic structure of the material's surface, which plays a pivotal role in determining the absorbate-surface bond strength and the occurrence of numerous catalytic and electrochemical reactions[19,20]. Positive strain applied to 2D material usually confers suitable adsorption energy upon the material, thus facilitating its desired development in electrochemical reactions, while unfavorable strain frequently results in subpar material performance. The primary objective of strain engineering of 2D materials lies in regulating the properties of 2D materials and optimizing the properties towards related devices through the application of tensile or compressive strain.

To date, various strategies have been implemented for generating strain to explore new physicochemical properties of 2D materials. The strain in 2D materials can be categorized into two types: internally generated and externally applied[21]. Internal strain is mainly generated by manufacturing local lattice distortion or interface interaction[22], including heteroatom doping, lattice vacancies, local lattice mismatch, heterostructure, *etc*. While external strain mainly involves external force or stimulation, such as substrate bending[23] and rigid substrates[24]. In comparison, internal strain exhibits greater stability and durability. However, it poses challenges in terms of control. On the contrary, external strain offers more precise controllability but relies on external force support. Once the external force is removed, the strain dissipates as well.

Compared with 3D bulk materials, 2D materials with ultrathin morphology have unique advantages in strain engineering. On the one hand, the high Young's modulus and excellent deformability of 2D materials ensure significant uniaxial or biaxial strain without fracturing. On the other hand, the electron cloud of 2D materials is confined to a 2D plane, rendering it more susceptible to external influences[25-27]. The local strain introduced into 2D materials stretches or compresses the nearby lattice, alters the microenvironment of atoms, and imparts completely different properties to the material. According to the d-band theory raised in 1998[28], the strain-induced variation of atomic distance can significantly influence the density of the d-state, which affects the adsorption performance of the material surface. For 2D materials, strain changes the atomic bond configuration (length and angle) and the interactions between the electron orbitals of adjacent atoms, thus adjusting the properties of 2D materials and providing a rich library for advanced applications[29-31].

So far, numerous methods have been developed for applying strain to 2D materials [Figure 1][32-43]. According to the source of strain, the methods for introducing strain can be roughly divided into three types: defect-induced, lattice-induced, and substrate-induced. There are different advantages and disadvantages among diverse strain introduction methods, which are suitable for diverse applications. For instance, defects can always trigger nonuniform microstrain, which is closely associated with the active site located on the material's surface, thereby potentially endowing the material with enhanced catalytic properties[19,21]. In contrast, substrate-induced strain provides uniform and continuously adjustable strain in the material. However, the removal of the substrate leads to an immediate change in internal strain. For lattice mismatch-induced strain, the compression of crystals possessing larger lattice parameters is concomitant with the stretching of crystals with smaller lattice parameters at the contacted interface,

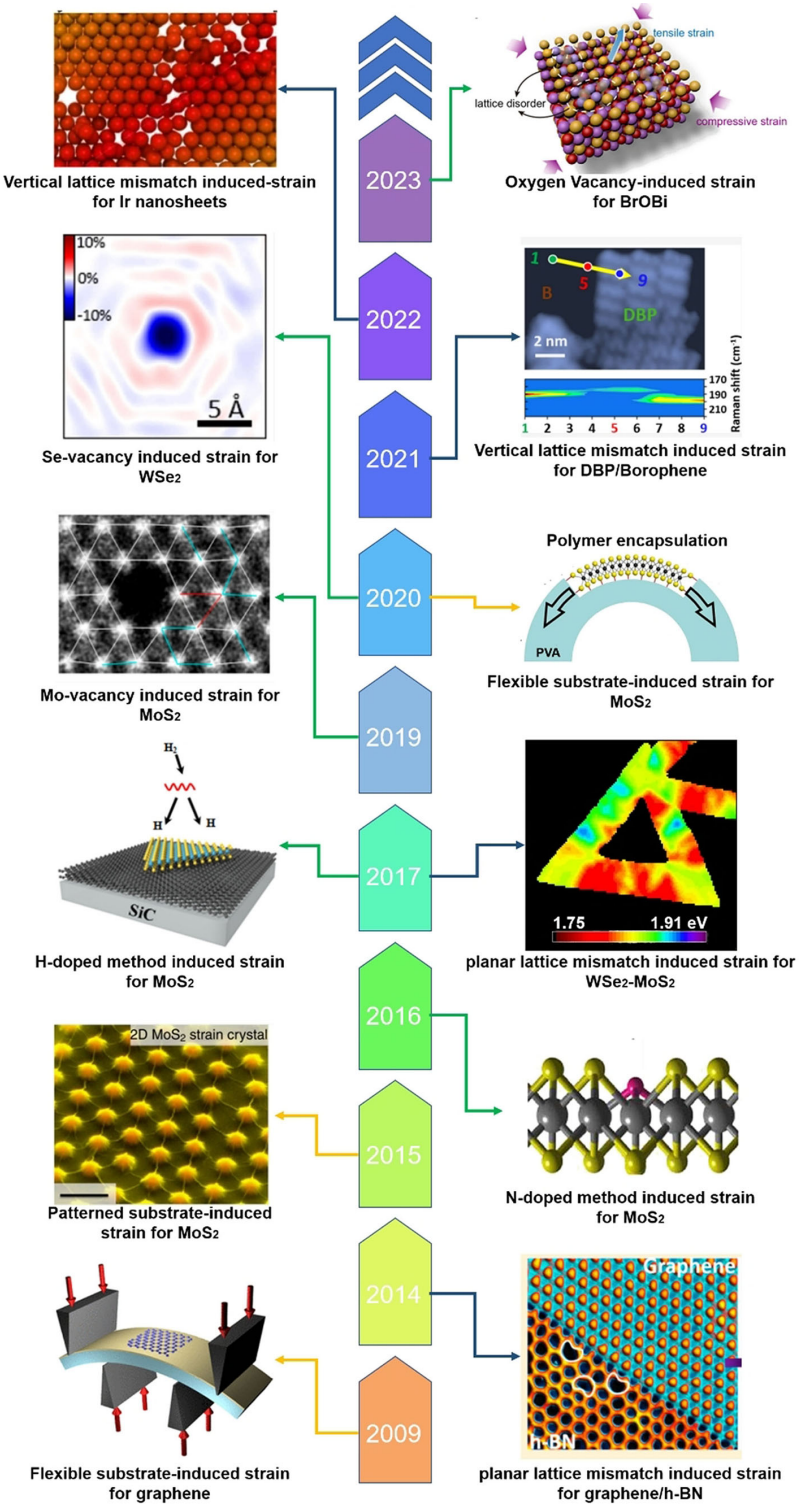

Figure 1. Development timeline of strategies for strain engineering of 2D materials. (2009): quoted with permission from Mohiuddin *et al.*[32]; (2014): quoted with permission from Lu *et al.*[33]; (2015): quoted with permission from Li *et al.*[34]; (2016): quoted with permission from Azcatl *et al.*[35]; (2017): the figure on the left is quoted with permission from Pierucci *et al.*; the figure on the right is quoted with permission from Hsu *et al.*[36,37]; (2019): quoted with permission from Yang *et al.*[38]; (2020): the figure on the left is quoted with permission from Lee *et al.*; the figure on the right is quoted with permission from Li *et al.*[39,40]; (2021): quoted with permission from Li *et al.*[41]; (2022): quoted with permission from Wu *et al.*[42]; (2023): quoted with permission from Cao *et al.*[43]. 2D: Two-dimensional.

resulting in a controllable interfacial strain type. However, determining the specific strain magnitude and location of the strain can be challenging[19].

Strain engineering is essential for tailoring the properties of 2D materials to meet specific requirements in various applications. In terms of energy storage, strain engineering of 2D materials shows a prospect of effectively reducing the diffusion barrier for mental ions, optimizing the adsorption model, and enhancing the material's diffusion kinetics. Simultaneously, strain engineering of 2D materials can mitigate volume expansion resulting from ion intercalation, which imparts enhanced stability and superior energy storage performance to the material[44,45]. For electrocatalysis, strain engineering of 2D materials shows the potential to modify the internal electronic states of surface atoms and optimize intermediate adsorption models, thereby significantly influencing the electrochemical reactivity in electrocatalysis[46-48]. While the perspective moves to photocatalysis, strain engineering of 2D materials presents a promising avenue for narrowing the bandgap, enhancing the separation of photogenerated carriers, and tuning the absorption, comprehensively improving the photocatalytic performance of materials[49].

Herein, this review provides a comprehensive overview of the latest advancements in strain engineering of 2D materials for energy storage and conversion applications. First, a brief introduction concerning the basic concept, characterization, and quantization of strain is delivered. Subsequently, different strategies for strain engineering of 2D materials are systematically summarized and compared, such as defect-induced, substrate-induced, and lattice mismatch-induced. Further, the recent applications of strain engineering of 2D materials in energy storage and conversion are discussed. Finally, we propose potential avenues and challenges for optimizing 2D materials by strain engineering.

FUNDAMENTAL UNDERSTANDING OF STRAIN IN 2D MATERIALS

Definition and characterization of strain in 2D materials

Among various material properties, strain holds significant importance in numerous fields, including materials science[50], chemistry[51], and molecular catalysis[19]. Correspondingly, different definitions and quantification methods for observed strain have been proposed for different fields and applications. For materials science, the local strain of 2D materials is usually defined as:

$$\varepsilon = (I_b - I_a)/I_a \quad (1)$$

where ⊠ represents the strain magnitude, and I_a and I_b represent the length of the atomic bond before and after the straining process, respectively. However, in practical applications, the strain within the material may not be uniform; it is not easy to evaluate atomic bond lengths and internal strain accurately and statistically (i.e., using large samples). Local strain measurement and global strain measurement are the two most frequently employed methods for measuring strain to simplify the strain model. Correspondingly, spectral measurement and microscopic visual measurement are two classical methods employed for the global and local identification of surface strain in 2D materials, respectively. Additionally, theoretical calculations also serve as a crucial supplement in verifying the strain in 2D materials.

For spectroscopy measurements, as phonon modes and band gaps of 2D materials exhibit sensitivity to strain, their change can be measured by Raman and photoluminescence (PL) spectra in practical applications[25,52]. Strain changes the crystal vibration and usually results in a change in phonon modes. Therefore, the strain inside the material can be easily characterized by monitoring the crystal vibration through Raman spectroscopy. For instance, Liu *et al.* conducted various spectroscopic analyses at different

regions of MoS_2/ZnO heterostructure arrays, and the maximum strain of approximately 0.6% was detected near the edge of ZnO nanorod[53]. Meanwhile, the band gap of the material is closely related to the internal strain, which can be reflected in the PL spectrum[39]. Conley *et al.* used PL spectroscopy to measure the optical band gap of MoS_2 and found that the PL shift exhibited an approximately linear relationship with strain[54]. In addition, X-ray absorption spectroscopy is also an effective way to characterize the strain. Di *et al.* used this technology to measure the Bi-Bi and Bi-O bond length inside the $Bi_{12}O_{17}Br_2$ nanoplates and nanotubes, and the variation in bond length indicated the tensile lattice strain in $Bi_{12}O_{17}Br_2$ nanotubes[55].

For microscopic visual measurements, the determination of materials' lattice spacing is typically achievable through high-resolution transmission electron microscope (HRTEM) lattice images[56], Through geometric phase analysis (GPA)[57], *etc*. By comparing the image features with the reference lattice, the local lattice spacing is explained as the component variation and strain. The GPA allows the evaluation of the degree of local lattice distortion in 2D materials, making the strain distribution visible in the form of strain mapping. Other characterization techniques that can be employed include spherical aberration corrected transmission electron microscope (ACTEM), scanning transmission electron microscopy (STEM), *etc.*

Theoretical calculations are another important method to simulate the strain effect and further verify the strain in materials. Zhang *et al.* calculated the bandgap of Nb-substituted WS_2 and found that this variant with lattice strain showed a bandgap consistent with the experimental results, suggesting the presence of lattice strain within the material[58].

Quantization of strain in 2D materials

As mentioned above, the measurements of strain encompass both local and global aspects, and different characterization methods correspond to distinct means of quantization. For local strain measurement, microscopic visual measurement has been widely used to determine the lattice spacing of materials. Image features are compared to the reference lattice using techniques such as cross-correlation, peak finding, or GPA, which enables precise atomic localization[19]. The local strain is quantified by comparing the lattice constants of the local atoms with the reference lattice. For instance, Yang *et al.* compared the bond length of the Mo-Mo bond near the Mo vacancy with the standard MoS_2 lattice and found that local strain of ~3% occurred in the surrounding atoms[38]. For global strain measurement, for instance, the Raman spectroscopy technique has proven to be an effective approach for characterizing and quantifying strain. There exist two formulas for computing strain in the material through Raman change:

$$\varepsilon = (\omega - \omega_0)/\chi \text{ or } \varepsilon = (\omega - \omega_0)/2\gamma\omega_0 \quad (2)$$

where the ω and ω_0 represent the Raman frequencies under detected strain and zero strain, respectively. The transfer rate of the χ is the Raman mode of vibration, and γ is the Grayson parameter[19,53]. Castellanos-Gomez *et al.* measured the Raman spectra on both the flat and top regions of the MoS_2 flake, both in-plane mode (E^1_{2g}) and out-of-plane mode (A_{1g}) on the top of the wrinkle, showing a redshift[59]. Based on the redshifted Raman spectrum, the maximum strain (tensile) is estimated to be 2.5%. For the strain in 2D materials on the elastic substrate, the strain exerted on the flexible substrate can be expressed by a simple equation:

$$\varepsilon = \tau/R \quad (3)$$

where τ and R represent the thickness and radius of curvature of the substrate, respectively. The radius of curvature can be calculated ideally as the substrate bends or shapes change[39].

CREATIONS OF STRAIN IN 2D MATERIALS

Atomically thin 2D materials have raised much attention for strain engineering due to their ultrathin characteristic and stronger deformation capacity than bulk materials[27,29]. With regard to strain, it can be generally divided into macrostrain and microstrain[60]. Macrostrain (also referred to as global strain in material science)[61] always refers to the distortion of the global crystal structure, accompanied by the global deviation of the lattice parameters from the perfect crystal. It induces a modification in the orbital overlap between adjacent atoms, leading to a shift of the d-band center and alterations in bonding energies with adsorbates. Microstrain, on the other hand, refers to the nonuniform strain effect caused by local deviations of atoms from their ideal positions. Since microstrain involves the local distortion of atoms, the introduction of microstrain brings more active sites to the material, which endows the material with better catalytic activity[60]. So far, the application of strain to 2D materials has been widely employed by various experimental methods and strategies (defect, lattice mismatch, substrate, *etc.*). This section provides a summary of various methods for introducing strain to 2D materials.

Defect-induced strain

On account of the ultra-thin characteristic of 2D materials, it provides an ideal platform for studying the strain effect caused by local defects[62]. In general, defect consists of point defects, line defects, planar defects, and body defects[63,64]. Local defects or lattice disorders in the material are always entangled with microstrain. In other words, microstrain represents the local deviation of an atom from its ideal position[60]. Meanwhile, the change of the relative position of atoms in 2D materials can induce compression or expansion among local lattice and manifests as the change of lattice constant. By comparing the deviation of the lattice constant between the lattice near the defect and the ideal lattice, the magnitude of the strain near the defect can be quantized. Since point defects (vacancies and dopants) are the predominant and most effortless type, we discuss them in detail in this section.

Doping-induced Strain

Doping, as a crucial type of point defects, can be classified into substitutional doping and interstitial doping. Regardless of the type of doping, it can cause the local deviation of nearby atoms from their ideal position, affect the bond length of the chemical bond, and bring microstrain to the local material[46,60]. Depending on the doping type and the size of each atom, local tensile and compressive strain can be generated near the doping site.

Plasma exposure is a widely used practical technique for incorporating heterogeneous atoms into 2D materials. Azcatl *et al.* utilized N_2 plasma to expose nitrogen (N) to MoS_2 for stable covalent doping [Figure 2A][35]. Due to the substitution of smaller N atoms with sulfur (S) atoms, the compressive strain was generated in the MoS_2 lattice. The Raman spectra for exfoliated N-doped MoS_2 flake displayed a blue shift of the (E^1_{2g}) mode, indicating compressive strain was generated due to the introduction of N atoms [Figure 2B]. In another work, Pierucci *et al.* reported the doping of atomic hydrogen (H) to a single layer of MoS_2 by exposing single-layer MoS_2 to a H_2 atmosphere[36]. The blue shift of (E^1_{2g}) mode in Raman spectra indicated the intercalation of H atoms and the occurrence of tensile strain.

Compared with plasma post-processing, introducing doping-induced strain during the synthesis is a simpler method. Zhang *et al.* synthesized Nb-doped WS_2 with various Nb concentrations via a chemical vapor deposition (CVD) method [Figure 2C][58]. The deviation of Nb atoms led to a deformation of the

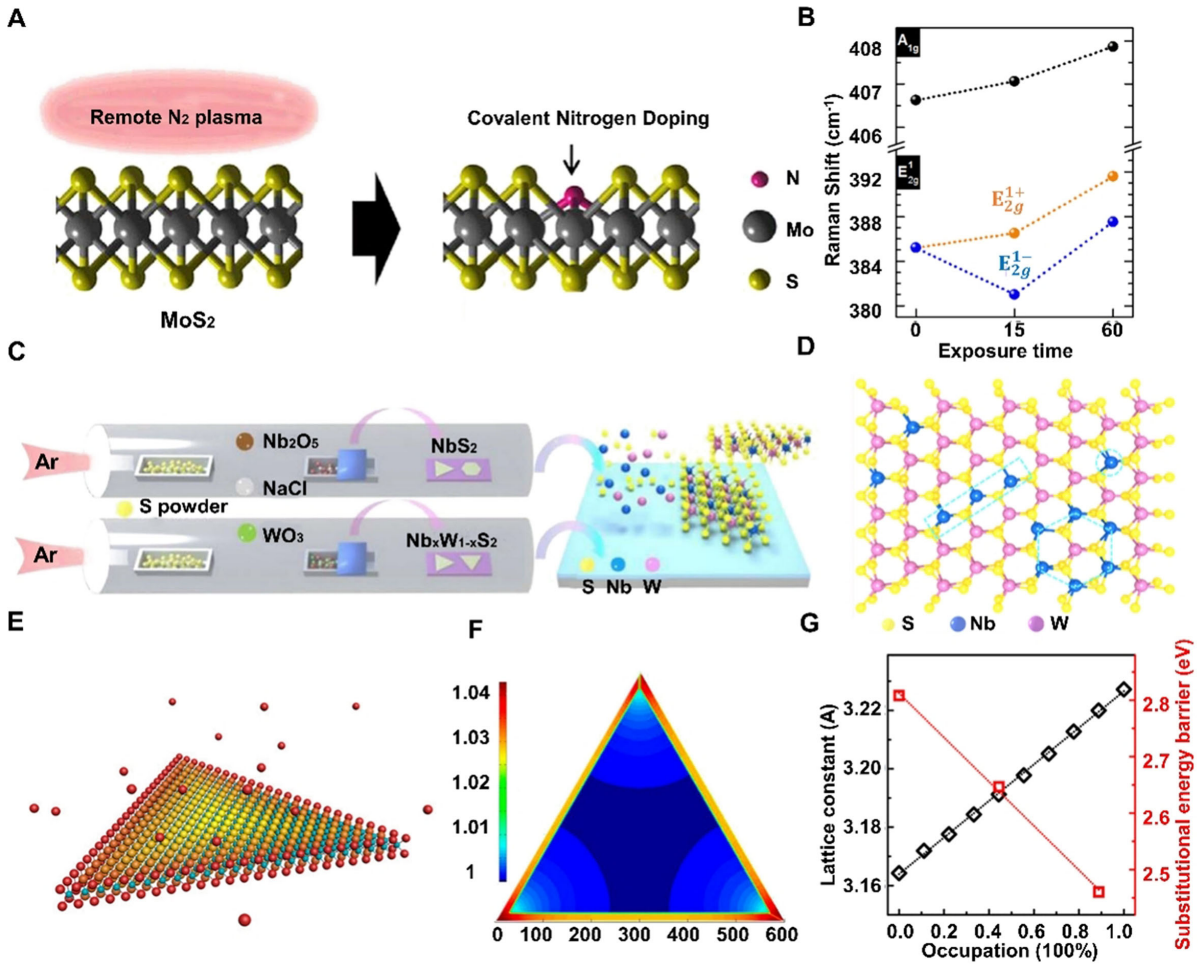

Figure 2. Doping-induced strain for 2D materials. (A) Schematic diagram of covalent nitrogen doping in MoS_2 via N_2 plasma treatment; (B) Raman shift after sequential N_2 plasma exposure for different times; (A-B): quoted with permission from Azcatl *et al.*[35]; (C) Schematic of the synthesis of NbS_2 and $Nb_xW_{1-x}S_2$ monolayers via a CVD method; (D) Atomic models of three doping configurations; (C-D): quoted with permission from Zhang *et al.*[58]; (E) Schematic of Se replacing S from the edge to the center in MoS_2; (F) Lattice constant at di erent positions as most of the outer S atoms are substituted by Se; (G) Calculation results illustrating the relationship among Se occupation, lattice constant, and substitution barrier; (E-G): quoted with permission from Li *et al.*[22]. CVD: Chemical vapor deposition; 2D: two-dimensional.

lattice and brought local tensile and compressive strain. A simple schematic diagram was shown to further reveal the internal structure of the material [Figure 2D]. Further, Li *et al.* reported the strain-driven mechanism of 2D atomic layered MoS_2 nanosheets [Figure 2E][22]. During the process of substitution of selenium (Se) with S in MoS_2, an increased lattice constant was observed at the edge, suggesting that the substitution occurred at the edge firstly. Theoretical calculation suggested a strong correlation between the substitution barrier and the local strain surrounding the substituted atom. The relaxation of strain at the periphery was easier than that in the inner region, resulting in a long-range strain field extending from the edge to the center [Figure 2F and G]. Moreover, doping-induced strain can also be observed in PdIr bimetallene[65], ZnO nanosheets[66], and nickel hydroxide nanosheets[67].

Vacancies-induced strain

Vacancies, another category of point defects in 2D materials, can be classified as cation and anion vacancies. In previous studies, it has been a challenge to differentiate vacancy and strain due to their entanglement[19].

The relationship between vacancies and strain can be summarized into three facets. First, vacancies can induce strain individually[40,68]. Regardless of the generation of cation and anion vacancies, they will induce local lattice compression and impose localized strain on the material[19,43]. As an illustration, Ni *et al.* demonstrated a linear correlation between oxygen vacancy (V_O) concentration and lattice strain at the Co-CoO interfaces[60]. Second, the interfacial strain can promote the generation of vacancies[69,70]. Third, strain and vacancy can coexist and act simultaneously. For instance, S vacancies and strain were introduced separately into MoS_2 nanosheets through argon plasma and capillary force[71]. As a result, under the synergistic effect of vacancy and strain, the material exhibited a promising property toward hydrogen evolution. In this part, our primary focus is on the strain induced by the introduction of vacancies.

Plasma treatment is a prevalent method for introducing vacancies and strains into 2D materials. For instance, atomic-scale vacancies were created into MoS_2 nanosheets through helium ion irradiation [Figure 3A][38]. As a result, multiple types of vacancies were observed (single and double S vacancies and Mo vacancies) [Figure 3B]. An enlarged image of high-angle annular dark field STEM (HAADF-STEM) near the Mo vacancy showed a deviation of ± 10 pm of Mo-Mo distance around the vacancy site, indicating that local strain of ~3% exists near the vacancy [Figure 3C]. In addition, vacancy-induced strain can also be introduced in numerous ways during the synthesis. Recently, Zhao *et al.* demonstrated a layered double hydroxide (LDH) with severely distorted structures and compressive strain [Figure 3D][68]. The K-edge EXAFS spectrum of Cr showed a decreased coordination number in CuCr nanosheets compared with CuCr-bulk, indicating that severe structure deformation and abundant V_O were formed [Figure 3E]. Similarly, Zhao *et al.* reported ultra-thin TiO_2 nanosheets with abundant V_O and compressive strain through Cu-doping strategies[72]. The substitution of copper for titanium caused a local charge imbalance and introduced additional V_O, while abundant V_O brought impressive compressive strain to the nanosheets. CVD is a crucial synthetic technique for inducing strain in 2D materials. For instance, a hexagonal monolayer WS_2 single crystal composed of alternating W vacancies (WVs) (β region) and S vacancies (SVs) (α region) was synthesized through CVD methods [Figure 3F][73]. The strain-related (E^1_{2g}) mode showed a blue shift around 0.1 cm^{-1} in the β region, indicating that the generation of WVs brought compressive strain to this region [Figure 3G].

Lattice mismatch-induced strain

In general, when two materials with different lattice parameters come into direct contact, lattice mismatch will occur at the interface, resulting in lattice strain in each component. The compressive strain occurs in the material with a larger lattice parameter, while the crystal with a smaller lattice parameter experiences tensile strain[74]. In the following, the lattice mismatch is divided into planar and vertical lattice mismatch, and the principle of strain introduction is discussed.

Planar lattice mismatch-induced strain

The planar lattice mismatch of 2D materials is invariably accompanied by the epitaxial growth of different materials. Researching the heterogeneous epitaxy and interfacial strain in various 2D materials has been a thriving research area for decades, owing to its technical relevance to solid-state devices and circuits[75]. Lattice-misfit strain in atomically abrupt lateral heterojunctions presents a novel approach for customizing their electronic properties.

The epitaxial growth of 2D materials with diverse lattice parameters will induce strain at the interface, which can be alleviated in the form of local lattice distortion. For instance, Lu *et al.* studied the strain propagation and relaxation mechanism at the interface of graphene/hexagonal boron nitride (h-BN) and found that an obvious sharp graphene/h-BN interface could be induced by forming a mismatch dislocation

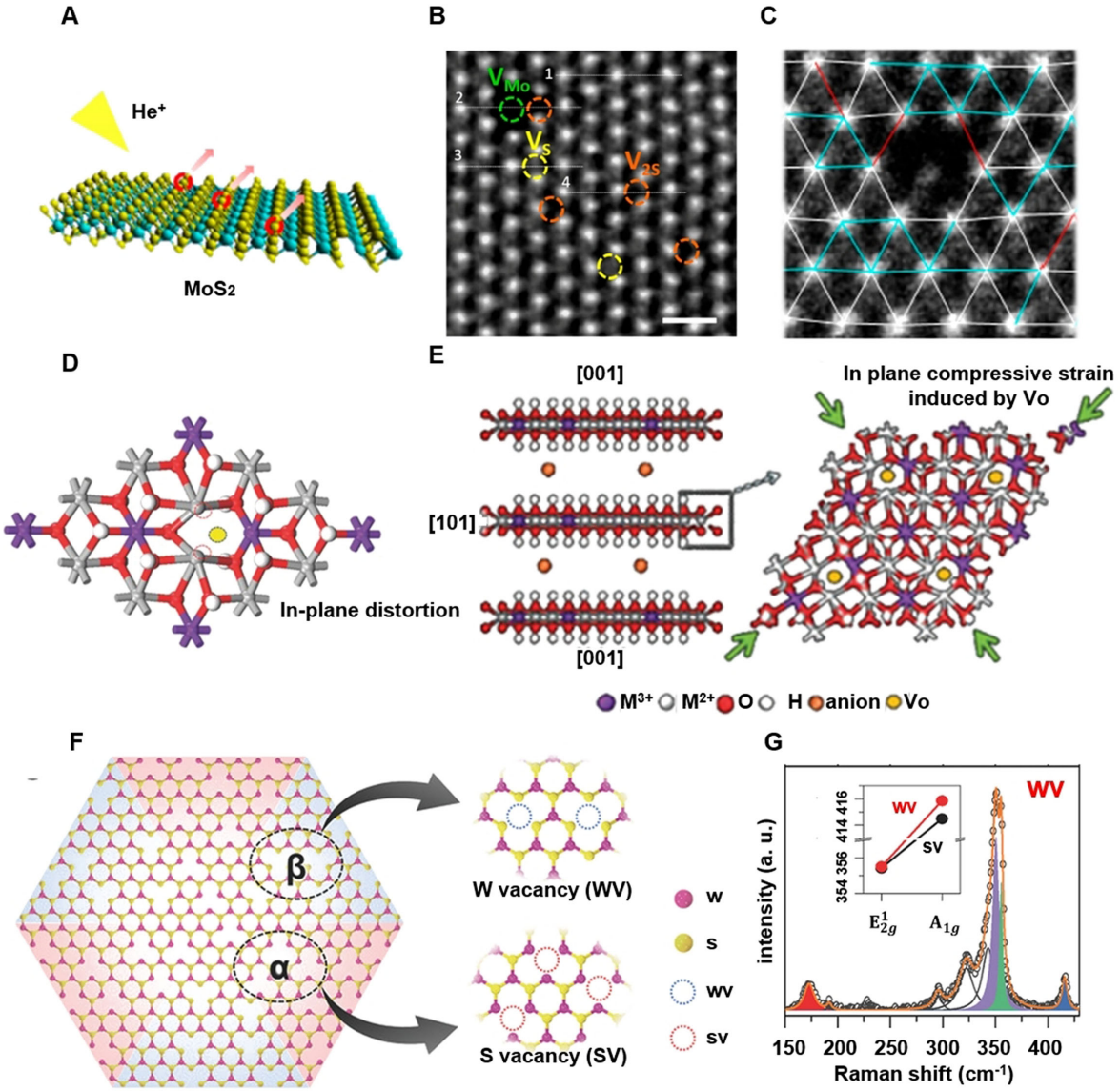

Figure 3. Vacancy-induced strain for 2D materials. (A) Schematic of MoS_2 basal plane irradiated with helium ions; (B) HAADF-STEM image of MoS_2 showing different types of vacancies; (C) Enlarged image of HADDF-STEM revealing the atomic structure in single layer MoS_2 near the vacancy site; (A-C): quoted with permission from Yang *et al.*[38]; (D) 2D structure model for LDH monolayer with V_O; (E) Schematic diagram illustrating the in-plane compressive strain induced by V_O in LDH nanosheets; (D-E): quoted with permission from Zhao *et al.*[68]; (F) Schematic illustrating the alternant domain of WVs and SVs in WS_2; (G) Raman spectrum for WV domains. Inset shows the frequency shifts for E^1_{2g} and A_{1g} modes; (F-G): quoted with permission from Jeong *et al.*[73]. HAADF-STEM: high-angle annular dark field scanning transmission electron microscopy; LDH: layered double hydroxide; SVs: S vacancies; WVs: W vacancies; 2D: two-dimensional.

at the interface to relieve the accumulated strain[33]. Li *et al.* presented a two-step epitaxial growth method for the formation of lateral WSe_2-MoS_2 heterojunction [Figure 4A][76]. The strain originating from the lattice mismatch is detected by Raman and PL variations. The adjacent MoS_2 exhibited a tensile state (cyan color) that gradually transitioned to a strain-free state (blue color). Some MoS_2 regions even exhibited compressive strain (red color) to relax the strain built upon the MoS_2 [Figure 4B]. Such a large strain difference caused by the planar heterostructure indicated the possibility of using strain to adjust the photoelectric properties of the material. Similarly, Hsu *et al.* studied the planar heterojunction of WSe_2-MoS_2 and found that it

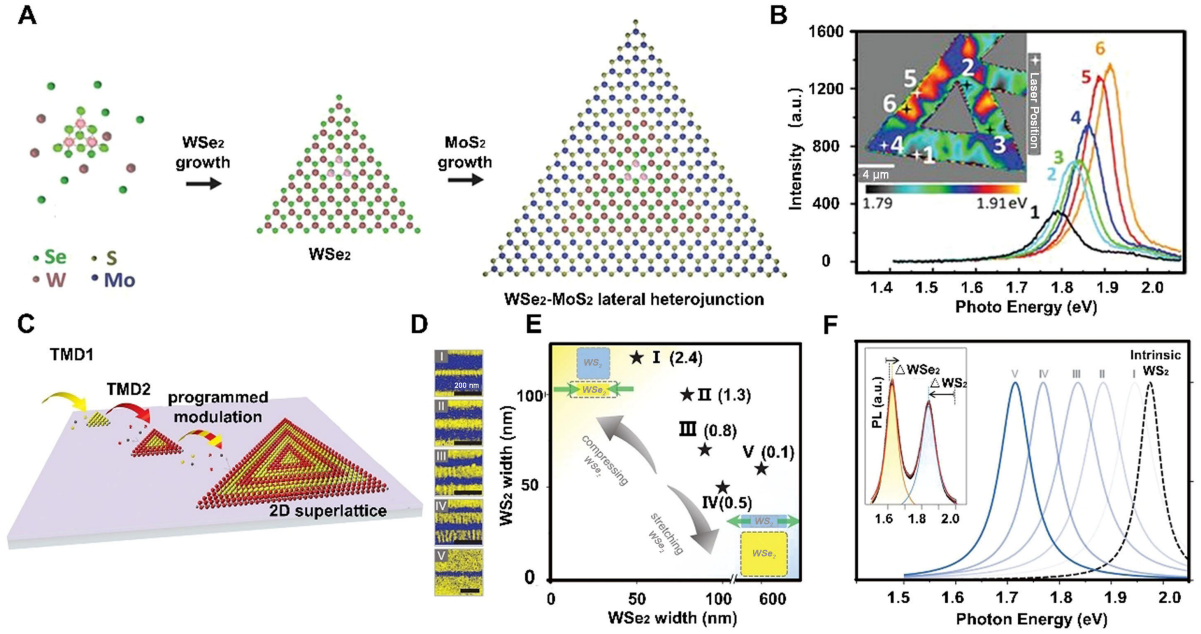

Figure 4. Planar lattice mismatch-induced strain for 2D materials. (A) Schematic illustrating the growth process of monolayer WSe_2-MoS_2 heterostructures; (B) PL spectra and its spatial mapping of MoS_2 at different locations; (A-B): quoted with permission from Li *et al.*[76]; (C) Schematic of 2D superlattices growth process composed of different TMDs; (D) False-color SEM images of a superlattice with different thickness configurations from I to V, Scale bars, 200 nm; (E) The plot of WS_2/WSe_2 superlattices with thickness configurations from I to V; (F) Normalized PL spectra of intrinsic WS_2 and WS_2 in the superlattices I to V; (C-F): quoted with permission from Xie *et al.*[77]. PL: Photoluminescence; TMDs: transition metal dichalcogenides; 2D: two-dimensional.

generated uneven strain in external MoS_2 through the PL peak surface scan map[37]. Further, Xie *et al.* reported an alternate transition metal dichalcogenide (TMD) monolayer composed of different compositions (e.g., WS_2 and WSe_2), which was achieved by carefully controlling the release and time of precursors during the growth [Figure 4C][77]. With the change of the thickness ratio of WS_2 and WSe_2 in planar superlattice, it was found that the lattice constant was determined by thicker layers. The different thickness ratios of WS_2 and WSe_2 layers brought different tensile and compressive strains on WS_2 and WSe_2 [Figure 4D and E] and further adjusted the magnitude of the direct band gap. As the thickness ratio of WS_2 to WSe_2 varied from 2.4 to 0.1 (I to V), the bandgap exciton resonance of WS_2 redshifted to a greater extent, which indicated the tensile (compressive) strain in WS_2 (WSe_2) [Figure 4F].

Vertical lattice mismatch-induced strain

Similar to the epitaxial growth of two different materials, the interaction of materials in the vertical direction can also cause a lattice mismatch, resulting in local strain[78]. Li *et al.* reported a vertical integration of borophene and tetraphenyldibenzoperiflflanthene (DBP) and revealed that compressive strain was induced to borophene underneath the molecular layer with tip-enhanced Raman spectroscopy [Figure 5A][41]. As the tip moved through the complete borophene (green spot), island edge (red spot), and absorbed borophene, different Raman shifts indicated distinct structure properties among different positions. The position far away from DBP exhibited a strong peak at 190 cm^{-1}, which corresponded to the characteristic of pristine borophene. The redshift at the island edge and the blue shift at absorbed borophene indicated compressive strain occurred at borophene underneath the molecular layer, while tensile strain occurred near the island edge [Figure 5B and C]. Further, Zhang *et al.* performed scanning tunneling microscopy (STM) imaging on the WSe_2-MoS_2 transverse heterojunction to map the full 2D strain tensor with a high spatial resolution. The moiré pattern resulting from the lattice mismatch between the underlying WSe_2 and MoS_2 was observed

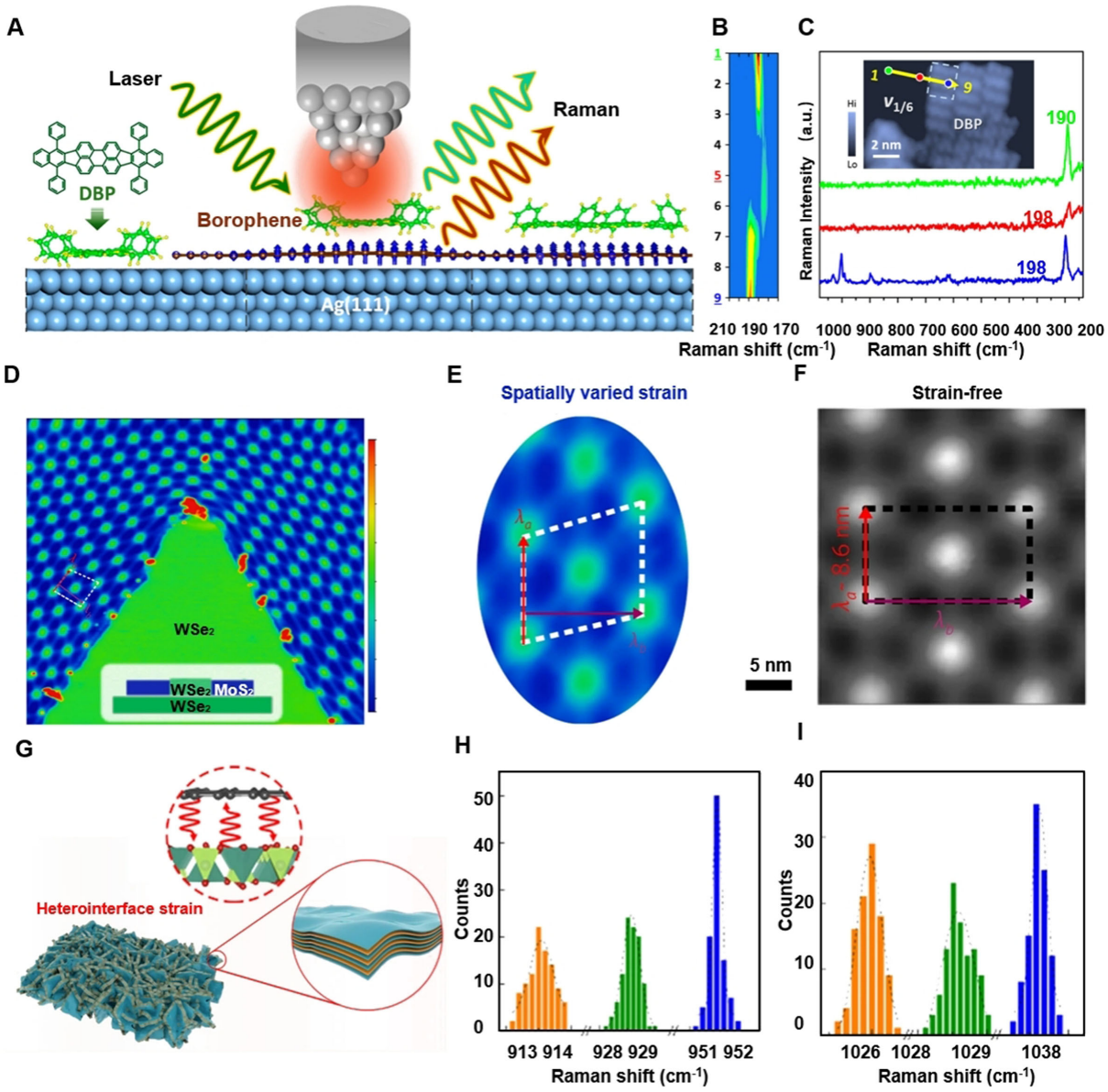

Figure 5. Vertical lattice mismatch-induced strain for 2D materials. (A) Experimental schematic diagram of TERS for Raman shift detection; (B) Spectral of 1D TERS measurements; (C) Tip-enhanced Raman spectroscopy was performed at the colored spots marked in the inset STM image; (A-C): quoted with permission from Li *et al.*[41]; (D) STM image of a transverse heterojunction of WSe_2-MoS_2; (E) An instance of the moiré pattern observed in a strain-free MoS_2/WSe_2 bilayer stack; (F) A close-up image of the moiré pattern in (D) shows spatially varying strains; (D-F): quoted with permission from Zhang *et al.*[79]; (G) Schematic diagram of the 2D multilayered $VOPO_4$-graphene heterostructure; (H-I) Distribution from 100 individual scans of $VOPO_4$-graphene heterostructures, showing the Raman shift of O-P-O and V=O (color orange indicates $VOPO_4$ nanoflakes, color green indicates $VOPO_4$-graphene, color blue indicates $VOPO_4{\cdot}2H_2O$); (G-I): quoted with permission from Xiong *et al.*[80]. STM: Scanning tunneling microscopy; TERS: tip-enhanced Raman spectroscopy; 2D: two-dimensional.

clearly [Figure 5D][79]. As a result, it produced tensile strain ε_{aa} = 1.17% in direction a and compressive strain ε_{bb} = 0.26% in direction b [Figure 5E]. For strain-free WSe_2-MoS_2, the moiré pattern appeared as a regularly arranged hexagonal superlattice with a fixed lattice constant that exhibited rotationally alignment [Figure 5F]. Our group synthesized a 2D multilayered $VOPO_4$-graphene heterostructure through interface strain engineering, which exhibited promising potential for energy storage beyond Li^+ ions (Na^+, K^+, Zn^{2+}, Al^{3+}) [Figure 5G][80]. Due to the mismatch of in-plane lattice distance between $VOPO_4$ and graphene,

significant interfacial strain propagates from the interface of $VOPO_4$-graphene to the $VOPO_4$ nanosheets. The Raman spectra over 100 times performed on the O-P-O and V=O mode showed a blue shift of ~15 cm^{-1} for O-P-O and ~3 cm^{-1} for V=O [Figure 5H and I], which indicated the interface strain between $VOPO_4$ and graphene.

Substrate-induced strain

Since ultra-thin 2D materials act as a thin plastic film, they can readily adhere to the substrate supporting them, and strain can be introduced through substrate modulation[25]. Compared with microscopic modulation methods (such as defect[13] and lattice mismatch[81]), macroscopic methods can be used to precisely adjust the properties of 2D materials by modifying the electron cloud and lattice structure via substrate engineering[25]. Flexible and rigid substrates have been utilized to modify the properties of 2D materials with more precision and controllability.

Flexible substrate-induced strain

Bending or stretching the substrate is a commonly utilized approach to induce surface strain in experimental settings, especially for flexible 2D materials. Due to the strong van der Walls interaction between the 2D material and substrate, the 2D material undergoes strain that is commensurate with the substrate, assuming that no interface slip occurs[82].

In early studies, a general approach to introduce strain is to place exfoliated 2D nanosheets onto a deformable substrate such as poly (ethylene terephthalate) (PET)[83], polydimethylsiloxane (PDMS)[84], poly(methyl methacrylate) (PMMA)[23], *etc*. For instance, Mohiuddin *et al*. used PET and acrylic films as a substrate for two-point and dour-point bending [Figure 6A and B][32]. The substrate was coated with photoresist to facilitate the identification of monolayer graphene on the substrate, followed by deposition of graphene layers prepared through micromechanical cleavage onto the substrates. The strong van der Walls interaction between graphene and the substrate ensured a synchronous deformation of the graphene layers with the substrate. This simple and effective approach facilitated the observation of a corresponding alteration in Raman spectra. Nevertheless, the interaction between 2D materials and the substrate was typically characterized by weak adhesion, which may leads to significant slippage during bending or stretching process and results in inefficient strain transfer[39]. In order to solve this problem, Huang *et al*. evaporated titanium to clamp the graphene onto the PDMS film[85], which prevented the slippage under mechanical force. In addition, Li *et al*. proposed a new approach involving polymer encapsulation to achieve effective strain transfer of 2D materials [Figure 6C and D][39]. First, monolayers of MoS_2 were transferred onto Si/SiO_2 substrates. Subsequently, a layer of polyvinyl alcohol (PVA) was applied via spin-coating to achieve complete encapsulation of MoS_2. The robust interaction force between the spin-coated PVA and 2D material ensured efficient transfer of mechanical strain, thereby minimizing the slippage or decoupling. Moreover, the variation of Raman and PL also confirmed that strain can be introduced to a greater extent compared with the traditional exfoliating method.

Besides, using the elasticity and piezoelectricity of the substrate is a commonly utilized technique for inducing strain to 2D materials. Castellanos-Gomez *et al*. created local strain in MoS_2 using prestretched elastomer substrates [Figure 6E][59]. At first, the elastomer base was prestrained. Then, the 2D material was deposited on the prestrained substrate. Wrinkles were formed in the MoS_2 layers when the substrate tension was released, and the buckling-induced delamination and uniaxial tensile strain were introduced in MoS_2. Hui *et al*. applied a bias voltage to a piezoelectric substrate to induce biaxial compressive strain in trilayer MoS_2. The shrink uniformly of the piezoelectric substrate subjected the trilayer MoS_2 to uniform compressive biaxial strain [Figure 6F][86]. In addition to these retractable substrates, heat-deformed liquid

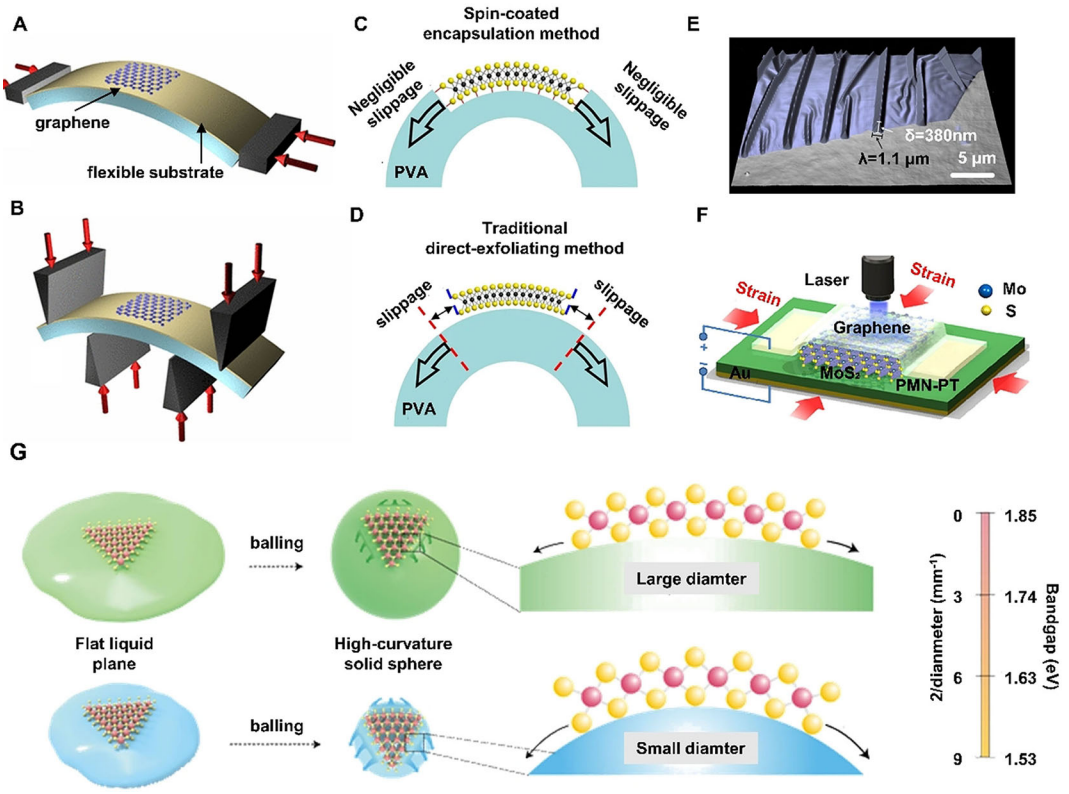

Figure 6. Flexible substrate-induced strain. (A-B) Scheme for bending tests with two and four points; a graphene monolayer is positioned on a SU8-coated substrate in the center; (A-B): quoted with permission from Mohiuddin *et al.*[32]; (C-D) Schematic diagram of fabrication methods of using PVA spin coating encapsulation and conventional direct exfoliation; (C-D): quoted with permission from Li *et al.*[39]; (E) AFM topography image of wrinkled MoS_2 flake created by buckling-induced delamination; quoted with permission from Castellanos-Gomez *et al.*[59]; (F) Schematic diagram of MoS_2 layers sandwiched between the piezoelectric substrate and graphene top electrode; quoted with permission from Hui *et al.*[86]; (G) Schematic illustration of the lattice deformation in MoS_2 on glass spheres with varying diameters; quoted with permission from Zeng *et al.*[87]. AFM: Atomic force microscopy.

glass could also serve as an alternative method for inducing strain into 2D materials. Zeng *et al.* developed a method to introduce strain *in-situ* for growing MoS_2 on spherical glass surfaces [Figure 6G][87]. MoS_2 was first synthesized via CVD on a liquid glass substrate at low temperatures. As the temperature rose gradually, the flat liquid glass turned into a ball of a certain diameter, and then the strain was determined by the linear correlation with the curvature of the sphere. The smaller the radius, the greater the degree of lattice distortion. Interestingly, the positive (negative) curvature achieved a corresponding decrease (increase) in the bandgap through the PL spectrum.

Rigid substrate-induced strain

Due to their ultra-thin characteristics, 2D materials exhibit remarkable flexibility in conforming to the surface morphology of various substrates. The strong interfacial adhesion between 2D materials and substrate can result in strain accumulation near the prominent region of the substrate surface[34,88]. The rigid patterned substrate is an effective way to periodically introduce strain into 2D materials. Compared to flexible substrates, rigid substrates allow for a controlled introduction of strain through modulation of array element size (height, width, *etc.*), providing a foundation for establishing the correlation between substrate morphology and material properties[25].

When a 2D material is deposited on a nanostructured substrate, local strain can be introduced into the deformation region caused by the interaction between the substrate and the 2D materials[89]. Zhang *et al.* investigated the deformation and strain of graphene on densely packed SiO_2 nanosphere arrays and revealed that the strain was amplified as the size of nanospheres reduced from 200 to 50 nm [Figure 7A][90]. Molecular dynamics simulations validated the identical microscopic structure and size-dependent strain behavior and unveiled that a stronger and nonuniform interaction force between smaller nanospheres and graphene led to larger strain [Figure 7B]. Similarly, Resebat-Plantey *et al.* investigated the strain domain of configuration with different configurations caused by state variation on a pillar array substrate[91]. As a result, a transition from the collapsed state to a suspended one occurred as the pillar pitch decreased and finally showed a low strain profile in the contact regions. Lee *et al.* discovered that the bandgap of graphene could be periodically modulated, which was realized by placing graphene on a nanostructured substrate[89].

In addition, making use of gas pressure difference is a common technique to introduce strain in 2D materials through patterned substrates. Lloyd *et al.* deposited a MoS_2 monolayer on a SiO_2 substrate with microcavities using CVD methods[92]. The microcavities were circular apertures with diameters of 5 μm and depths ranging from sub-micrometer to a few micrometers [Figure 7C]. The sample was subjected to high-pressure conditions in a chamber (P_0) for an adequate duration, allowing the gas to permeate into the cavity that initially contained air at a pressure of 1 atm [Figure 7D]. When the internal pressure within the cavity reached P_0, the sample was taken out of the chamber. The pressure differential between the ambient air and internal pressure caused inflation of the MoS_2 layer and resulted in strain on MoS_2.

Further, Tomori *et al.* devised a method for introducing strain in graphene by constructing a patterned substrate with dielectric nanopillars[93]. First, graphene was placed on a Si substrate coated with lift-off resist (LOR). Then, an excess dose of e-beam was irradiated on the partial region; the exposed LOR was insoluble, while the unexposed LOR was removed by soaking it with N-methyl-2-pyrrolidone (NMP), nonuniform strain in graphene was introduced in this process. This approach is applicable to various 2D materials, and the strain distribution can be tailored by controlling the morphology of the supporting nanopatterns. Based on the previous work, Liu *et al.* employed a PMMA-assisted wet transfer approach to optimize the strain transfer from the substrate to 2D materials [Figure 7E][53]. The procedures were as follows: The ZnO substrates were patterned using electron beam lithography techniques. After, the MoS_2 nanosheets grown *in-situ* were precisely transferred onto ZnO nanorod arrays via a PMMA-assisted wet transfer method. Finally, the hybrid structures were immersed in acetone for PMMA removal and subsequently dried with a critical point dryer to eliminate residual acetone. The PMMA-assisted MoS_2 was drawn down by capillary force generated by water evaporation within the spacing of ZnO nanorods, followed by removal of PMMA with acetone. As a result, the biaxial strain was localized near the ZnO nanorods at the van der Waals interfaces [Figure 7F].

Comparison of different strategies for strain engineering of 2D materials

In the above content, we have provided a systematic description and classification of experimental strategies for creation of strain in 2D materials, along with an analysis of the characteristics associated with each method. To facilitate a more intuitive comparison between different strain induction techniques, Table 1 presents the range and types of strains achievable in various 2D material systems. This comprehensive summary enables researchers to identify the most suitable approach based on their specific research needs.

STRAIN ENGINEERING OF 2D MATERIALS FOR ENERGY STORAGE AND CONVERSION APPLICATIONS

The utilization of 2D materials presents both technological opportunities and novel fundamental insights

Table 1. Summary of the technique, type, and range of the strain for different 2D materials

Strain technique	Materials	Type of strain	Range	Ref.
Flexible substrate	Graphene	Uniaxial homogeneous	0%-1.3%	[32]
Planar lattice mismatch	Graphene/h-BN	Uniaxial inhomogeneous	1.9%-5.9%	[33]
Rigid substrate	MoS_2	Local inhomogeneous	0%-3%	[34]
Doping	MoS_2	Local inhomogeneous	0%-1.7%	[35]
Doping	MoS_2	Local inhomogeneous	-	[36]
Planar lattice mismatch	WSe_2/MoS_2	Uniaxial inhomogeneous	0%-2%	[37]
Vacancy	MoS_2	Local inhomogeneous	~3%	[38]
Flexible substrate	MoS_2	Uniaxial homogeneous	0%-1.49%	[39]
Vacancy	WSe_2	Local inhomogeneous	4.8%-8%	[40]
Vertical lattice mismatch	DBP/Borophene	Biaxial inhomogeneous	~0.6%	[41]
Vertical lattice mismatch	AC-Ir NSs	Biaxial inhomogeneous	~4%	[42]
Vacancy	BiOBr	Local inhomogeneous	5%-10%	[43]

AC-Ir NSs: Amorphous-crystalline Ir nanosheets; DBP: tetraphenyldibenzoperiflflanthene; h-BN: hexagonal boron nitride; 2D: two-dimensional.

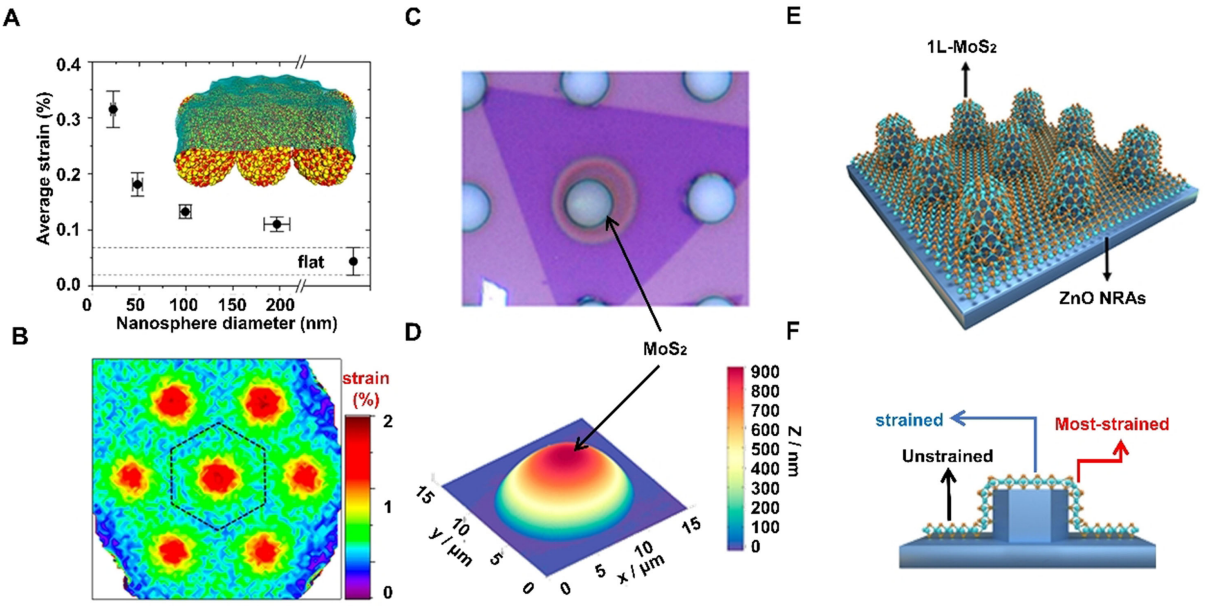

Figure 7. Rigid substrate-induced strain. (A) The average areal strain of graphene on top of the different central spheres; (B) Strain profiles of graphene on the top of 20 nm nanospheres; (A-B): quoted with permission from Zhang *et al.*[90]; (C) Microscope image of a MoS_2/SiO_2 substrate delaminated device (scale bar is 5 μm); (D) AFM image of MoS_2 in figure C; (C-D): quoted with permission from Lloyd *et al.*[92]; (E) Schematic diagram of the 1L-MoS_2/ZnO heterostructure arrays; (F) Strain distribution analysis of 1L-MoS_2 heterostructure on patterned ZnO substrate across various regions; (E-F): quoted with permission from Liu *et al.*[53].

for energy storage and conversion. The engineering of strain in 2D materials presents boundless opportunities for the design and regulation of their properties across various fields[94-96]. In the following, the basic applications of strain engineering in energy storage and conversion of 2D materials are summarized.

Strain engineering of 2D materials for energy storage

Two-dimensional materials stripped from their layered precursors have attracted great attention due to their huge surface area and easy modification properties[97-100]. As a widely reported method in electronics, strain engineering represents an efficient and straightforward method to manipulate the 2D materials[101-104].

In terms of energy storage, strain acts on material, engineering absorption, diffusion[105], and electrochemical reactivity[106], resulting in a reduced barrier for the diffusion and reaction of metal ions, minimizing energy loss and enhancing the material's performance in energy storage. Furthermore, during the intercalation process of metal ions for energy storage, the material always undergoes detrimental irreversible expansion, leading to poor cycling performance[107]. The introduction of appropriate interfacial strain can confer robust structural stability to the material during both the insertion and stripping of metal[80,108,109], thereby improving its overall energy storage capabilities. The application of strain engineering in energy storage is summarized below.

Regulating the electrochemical reactivity

The strain within the material can cause structural changes in the electron cloud, leading to alterations in both diffusion barrier and metal ion adsorption and imparting diverse energy storage properties to the material. For instance, Hao *et al.* demonstrated the tunability of Li/Na adsorption and storage in 2D MoS_2 through strain engineering via first-principles calculations[105]. The result suggested that proper tensile strain could increase the absorption of energy for Li/Na ions, influence the diffusion batteries, and narrow the semiconducting gap of MoS_2, thus leading to enhanced stability and improved electrical conductivity. In another work, Chen *et al.* suggested that the diffusion path of lithium atoms could be efficiently modified by uniaxial strain due to the variation in asymmetric surface geometry and electron polarization[110]. Further, Oakes *et al.* demonstrated that strain engineering at the interface of carbon-MoS_2 (C-MoS_2) heterostructure could guide the chemical storage pathway during lithium metal insertion into MoS_2 [Figure 8A][106]. Raman spectroscopy was conducted on both pristine MoS_2 nanosheets and interface-strained MoS_2 nanosheets at various cathodic potentials to elucidate the mechanism of lithium insertion. As cathodic potential scanned from open-circuit voltage to 0.01V, a distinct Raman peak emerged from the stacked C-MoS_2 nanosheets at a potential of 1.75V, while no change was observed in the Raman spectroscopy of pristine MoS_2 nanosheets under the same conditions, indicating the generation of lithium polysulfides [Figure 8B and C]. As the open circuit voltage continued to decrease, the signature of lithium polysulfides appeared at cathodic potentials as low as 0.01 V [Figure 8D], indicating a distinct reaction pathway and the same final product. Moreover, the normalized differential capacity curves of vertically stacked C-MoS_2 nanosheets and MoS_2 exhibited distinct chemical pathways during lithium insertion, which can be attributed to interface strain [Figure 8E and F]. This study demonstrated the potential of strain engineering in regulating energy storage pathways and underscored the significance of mechanical strain in material-based energy storage processes.

Relieving the volume change

Relieving the volume change caused by metal ion intercalation through strain engineering can enhance cycling stability and reversibility of the material during energy storage. Guided by this, an xDA-Ti_3C_2 with special pillar and strain structures was prepared through the reaction between xDA molecules and -NH_2 functionalized Ti_3C_2 through Liu *et al.* The unique strain structure of xDA-Ti_3C_2 relieved the volume change and maintained structural stability during ion insertion/extraction[109]. In addition, our group proposed a reversible intercalation mechanism for K^+ ions in the zero-strain 2D multilayered heterostructure cathode [Figure 8G]. Due to the disparity in lattice spacing between $VOPO_4$ and graphene, the interface-induced compressive strain was generated on $VOPO_4$ nanosheets, which relieved the expansion brought by the insertion of K^+ ions[80]. A reversible change in interlayer distance of $VOPO_4$-graphene layered cathodes during the charge/discharge process was demonstrated through *in-situ* X-ray diffraction (XRD) measurements, indicating a promising potential for energy storage applications [Figure 8H and I]. Benefiting from its alternating stack structure and interface strain between $VOPO_4$ and graphene nanosheets, the $VOPO_4$-graphene multilayered heterostructures exhibited a superior cycling and rate capability performance compared to bulk $VOPO_4 \cdot 2H_2O$ and restacked $VOPO_4$ [Figure 8J and K].

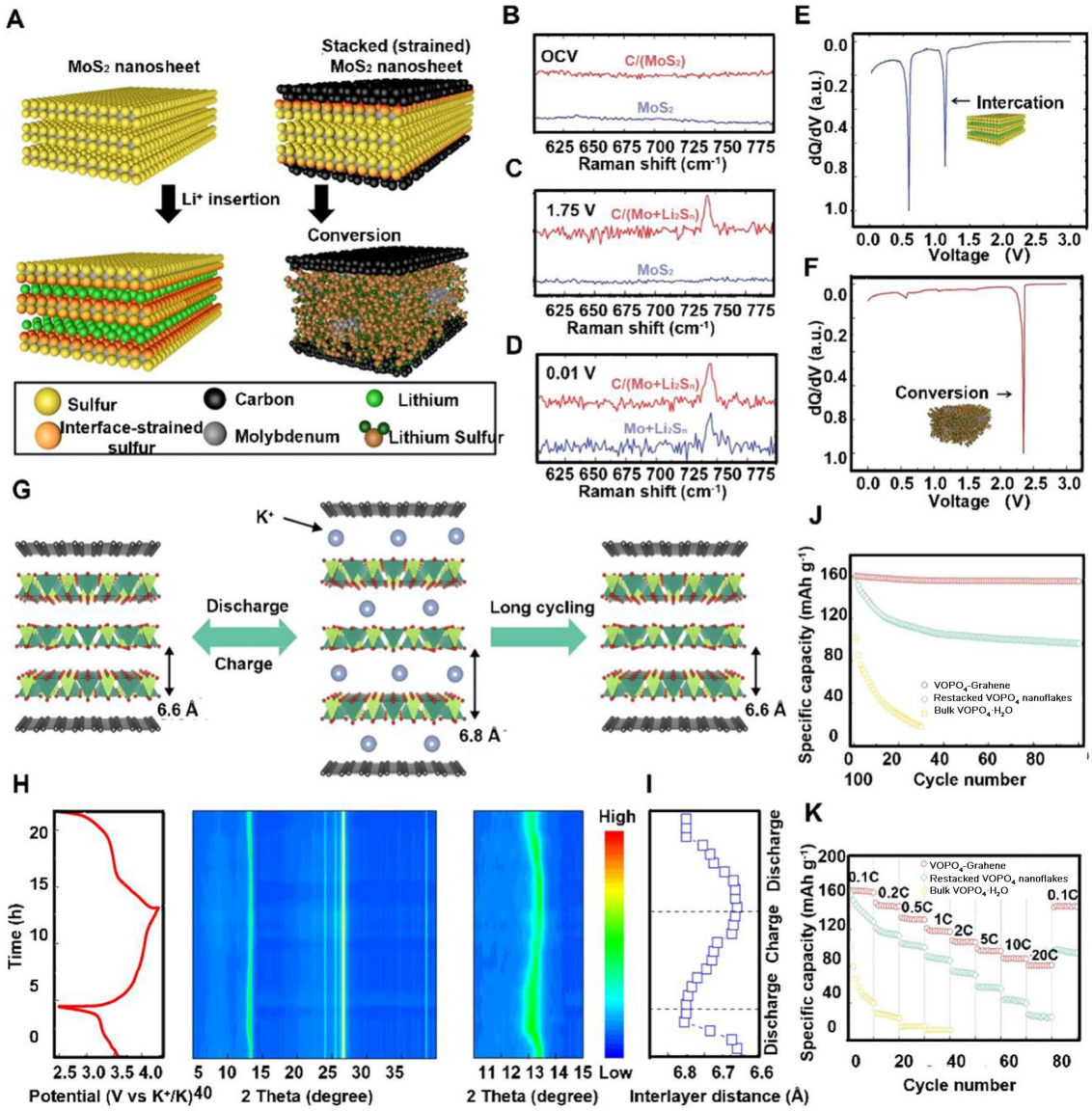

Figure 8. Strain engineering on energy storage and its mechanism analysis. (A) Schematic showing the different chemical reaction pathways of the nanosheets. *Ex-situ* Raman spectroscopy reveals different electrochemical signatures based on the Raman of polysulfides for pristine MoS_2 and interface-strained MoS_2 at (B) OCV, (C) 1.75V and (D) 0.01 V. Normalized differential capacity measurement for MoS_2 (E) and vertically stacked C-MoS_2 nanosheets (F), with two arrows indicate the potential of direct chemical conversation and intercalation reactions; (A-F): quoted with permission from Oakes *et al.*[106]; (G) Schematic illustration of the reversible intercalation mechanism of K^+ ions in 2D $VOPO_4$-graphene multilayer heterostructures; (H) Charge and discharge profiles of $VOPO_4$-graphene cathodes for K^+ ion batteries and corresponding *in-situ* XRD patterns; (I) The interlayer spacing of $VOPO_4$-graphene calculated from the XRD pattern during the process of charge and discharge; (J) Comparison of cycle performance of $VOPO_4$-graphene heterostructure, restacked $VOPO_4$ nanoflakes, and bulk $VOPO_4{\cdot}2H_2O$ at 0.1 C; (K) Rate capability comparison of $VOPO_4$-graphene heterostructure, restacked $VOPO_4$ nanoflakes, and bulk $VOPO_4{\cdot}2H_2O$ at various current densities from 0.1 to 20 C; (G-M): quoted with permission from Xiong *et al.*[80]. OCV: Open-circuit voltage; XRD: X-ray diffraction; 2D: two-dimensional.

Strain engineering of 2D materials for photocatalysis

In recent years, 2D ultra-thin nanosheets have shown great potential in the development of novel semiconductor photocatalysts. Benefiting from their ultra-thin morphological characteristics and abundant surface defects, a large amount of unsaturated metal sites are exposed, providing abundant adsorption for the reactants[111,112]. Photocatalysis can be defined as the process in which light interacts with a

semiconductor, and the generated electrons and holes induce a targeted redox reaction on the surface of the catalysts[49,113,114]. Photocatalysis involves four steps: (1) light absorption; (2) generation of electron-hole pairs; (3) transport of the photogenerated charge carriers from bulk to surface; and (4) catalysis on the surface of materials[115]. Strain engineering of 2D materials shows the potential to manipulate the band structure, enhance the separation efficiency of photogenerated electron-hole pairs, regulate intermediate absorption, and synergistically improve photocatalytic activity.

Regulating the band structure

Strain engineering is considered a highly effective way of regulating the bandgap and band position of materials, promoting efficient solar energy capture and enhancing the redox reactivity of photogenerated carriers[116]. As early as 2012, Feng *et al.* demonstrated a continuous band regulation of monolayer MoS_2 nanosheets under biaxial tensile strain[117]. Furthermore, Pak *et al.* observed that the direct-to-indirect bandgap in WS_2 can be induced by compressive strain[118]. Furthermore, Feng *et al.* manipulated the photocatalytic performance of BiOBr nanosheets in dye degradation and found that strain can modify the band structure of BiOBr[56]. Both tensile and compressive strain could lead to a narrowed bandgap of BiOBr nanosheets. In another work, a lepidocrocite-phase 2D TiO_2 sheet with crumpled morphology and nonuniform strain was synthesized via a one-step solvothermal methodology[119]. STEM images revealed the significant nonuniform strain, and lattice distortion was observed in different parts of the crumpled sheet, with compressive strains of 4% and 20% along the a and b axes, respectively. The valence band (VB) analysis calculated for strained/ unstrained 2D lepidocrocite TiO_2 showed that the theoretical band gap of strained titanium dioxide (1.80 eV) was in good agreement with the experimental value (1.84 eV), which was significantly smaller than the unstrained band gap (4.7 eV). The result indicated that the surface strain of lepidocrocite TiO_2 significantly enhanced the light absorption of both visible and near-infrared light.

Enhancing the carrier separation

Apart from the material's light absorption property, its excellent carrier separation capability also plays a crucial role in achieving high photocatalytic performance. Di *et al.* successfully synthesized $Bi_{12}O_{17}Br_2$ nanotubes as a photocatalyst for CO_2 reduction[55]. The tensile strain of the curved $Bi_{12}O_{17}Br_2$ nanotubes was approximately 5.5%. The surface tensile strain led to an increase in carrier separation and a better absorption model for CO_2. As a result, the CO_2 reduction performance of the nanotubes was enhanced by tensile strain tuning, surpassing that of $Bi_{12}O_{17}Br_2$ nanoplates (14.4 times). Further, Liang *et al.* reported lattice-strained nickel hydroxide nanosheets via a V-doped strategy for CO_2 reduction [Figure 9A][67]. The chemisorption profile of 10% V-doped $Ni(OH)_2$ nanosheets showed a higher temperature shift, indicating an increased number of exposed sites available for CO_2 adsorption and activation [Figure 9B]. The reduction in PL intensity after the introduction of vanadium (V) implied that surface strain on $Ni(OH)_2$ was conducive to the separation of photogenerated electron-hole pairs [Figure 9C]. Benefiting from the lattice strain and enhanced carriers' separation, the optimized $Ni(OH)_2$ nanosheets demonstrated the highest CO yield and the best selectivity [Figure 9D]. Even in a diluted CO_2 (0.1 atm) concentration, the lattice-optimized $Ni(OH)_2$ exhibited a remarkable CO generation of 3.5 $\mu mol \cdot h^{-1}$, which was superior to that of pure $Ni(OH)_2$ [Figure 9E]. The nearly identical Ni K-edge position before and after the reaction indicated that the original lattice strain structure was retained. [Figure 9F]. In another case, Hsu *et al.* reported a reversible photochromic BiOBr nanosheet, which exhibited excellent photocatalytic activity toward the coupling and oxidation of ethylbenzene. The presence of defects on the material surface induced lattice distortion in the nanosheets, leading to overall lattice strain in the structure. Theoretical calculation suggested that the lattice strain enhanced the probability of photocarrier transition and separation, thus facilitating hydroxyl radical generation and significantly improving the photocatalytic efficiency of C-H bond activation[37].

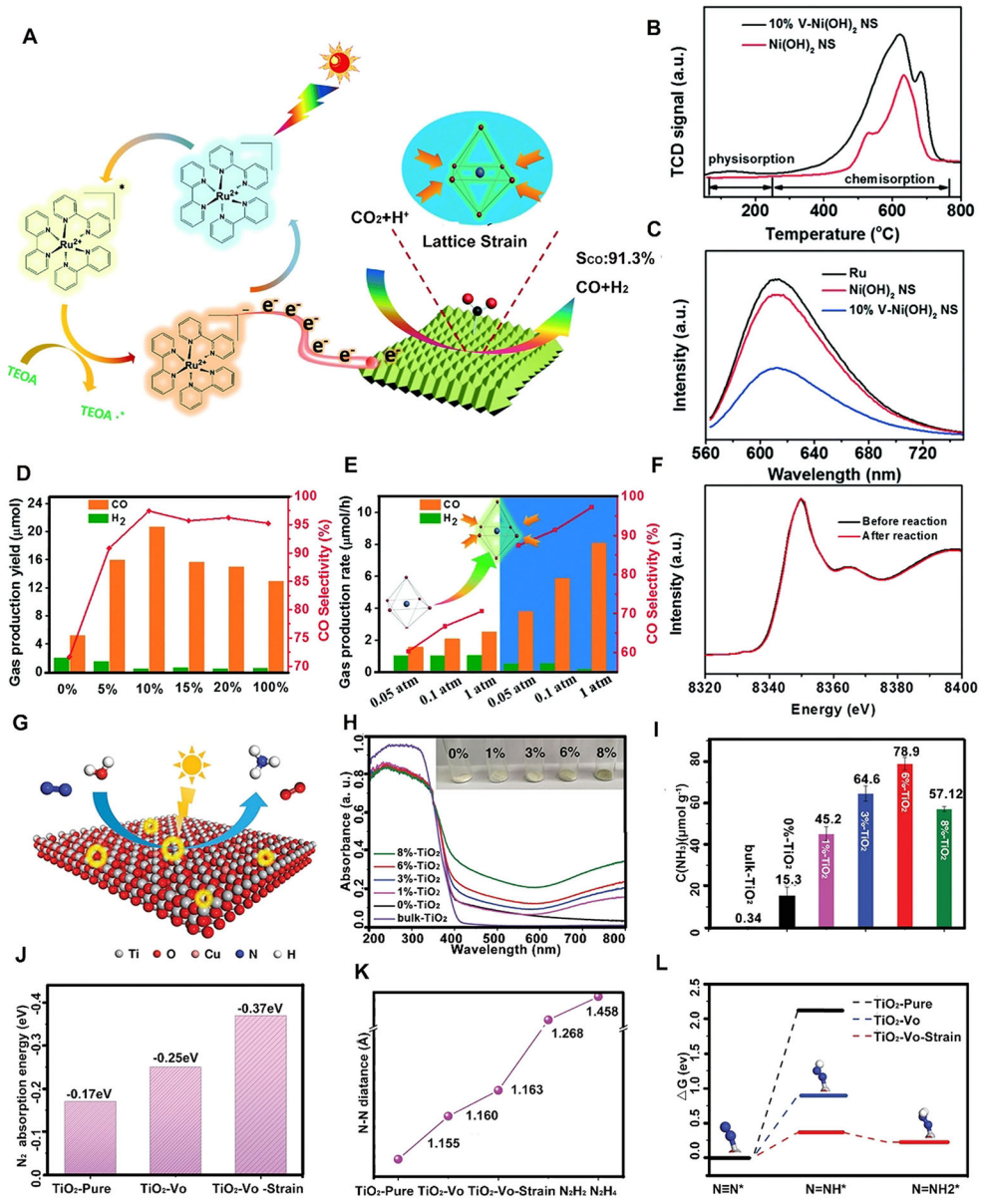

Figure 9. Strain engineering on photocatalysis and its mechanism analysis. (A) Proposed mechanism for photocatalytic CO_2 reduction using lattice-strain optimized $Ni(OH)_2$ nanosheets; (B) and (C) CO_2-TPD and PL spectra plots of $Ni(OH)_2$ nanosheets and 10% V-doped $Ni(OH)_2$ nanosheets; (D) The gas production yield and CO selectivity of x% V-$Ni(OH)_2$ nanosheets were evaluated under a pure CO_2 atmosphere; (E) CO_2 photo reduction performances of 10% V-$Ni(OH)_2$ nanosheets and $Ni(OH)_2$ were evaluated under varying CO_2 concentrations within the first hour; (F) Comparison of Ni K-edgeXANES spectra of 10% V-$Ni(OH)_2$ nanosheets before and after the reaction; (A-F): quoted with permission from Liang *et al.*[67]; (G) Schematic photocatalytic process of N_2 fixation on the surface of ultrathin TiO_2 nanosheets with V_O and engineered strain; (H) UV-vis diffuse reflectance spectra for Bulk-TiO_2 and the x%-TiO_2 nanosheets (contain x% mol Cu); (I) Yield of NH_3 of different samples after UV-vis illumination for 1h with water as the proton source; (J) The calculated adsorption energies of N_2 on TiO_2-Pure, TiO_2-V_O, and TiO_2-V_O-Strain; (K) N-N distance of N_2 on TiO_2-Pure, TiO_2-V_O, TiO_2-V_O-Strain, N_2H_2, and N_2H_4; (L) The free energy diagram depicting the N_2 fixation process on the surface of TiO_2-Pure, TiO_2-V_O, and TiO_2-V_O-strain; (G-L): quoted with permission from Zhao *et al.*[72]. PL: Photoluminescence; TPD: temperature programmed desorption; XANES: X-ray absorption near edge structure; UV-vis: ultraviolet-visible.

Tuning the absorption and optimizing the reaction path

The photocatalytic performance of the material is closely correlated with the absorption and desorption of intermediate products during the reaction. Strain engineering of 2D materials exhibits potential in

optimizing intermediate product absorption through a low-energy pathway for the final reaction. Zhao *et al.* reported a co-precipitation method to enhance the chemisorption and activation of N_2 through strain engineering[68]. Density function theory (DFT) calculations indicated that vacancy-introduced strain modified the gap state and enhanced the absorption and activation of H_2O and N_2. As a result, it endowed an excellent photocatalytic activity for converting N_2 to NH_3. Zhao *et al.* reported a facile copper-doping strategy for synthesizing ultrathin TiO_2 nanosheets with V_O-induced compressive strain for photocatalytic nitrogen fixation [Figure 9G][72]. A large amount of V_O could be induced to TiO_2 nanosheets with the doping of Cu to achieve local charge balance, thus introducing compression strain. As a result, the compressive strain-optimized TiO_2 nanosheets showed superior light absorption [Figure 9H], and 6%-TiO_2 exhibited an optimum performance for N_2 fixation in water [Figure 9I]. Further DFT calculations suggested that the adsorption of N_2 was most favorable on the surface of TiO_2 nanosheets with V_O and compressive strain [Figure 9J]. The increased absorption to N_2 facilitated the charge transfer between TiO_2 and N_2 and weakened the N-N bond [Figure 9K]. Various Gibbs free energy diagrams for nitrogen fixation indicated that the sluggish Volmer step on TiO_2 could be significantly accelerated after the introduction of strain [Figure 9L], leading to an enhanced N_2 activation and fixation performance.

Strain engineering of 2D materials for electrocatalysis

Noble metals exhibit superior electrocatalytic performance. However, their limited reserves and high costs have prompted the exploration of alternative options[46,120,121]. Two-dimensional materials have garnered significant attention in the realm of electrocatalysis due to their unique characteristics, such as ultrathin morphology, fully exposed surface atoms, and exceptional mechanical properties[122]. Their application in electrocatalysis has been further expanded through strain engineering to achieve various properties. Electrocatalysis refers to the process in which the intermediate adsorbed on the catalyst surface undergoes oxidation-reduction reactions and desorption to produce the target product under the influence of electricity[123]. A proper adsorption ability between the intermediate and the catalyst surface plays an essential role in the electrocatalytic reaction. According to the d-band theory raised in 1998[25], the d-band center typically undergoes variations in response to the change in the local coordination environment surrounding metal atoms. As a result, compressive lattice strain will cause an increased overlapping of the d-orbitals of metal atoms. This overlap will increase the bandwidth and lower the d-band center energy, pushing more antibonding states below the Fermi level and allowing adsorbates to interact with them, which weakens the binding energy of adsorbates. On the contrary, tensile lattice strain shows the opposite effect. The change in atomic distance induced by strain can significantly impact the electron density of the d-state and enhance electrochemical activity on material surfaces[124-126]. The application of strain on 2D materials induces additional lattice irregularities, thereby optimizing the adsorption energy for intermediate products and boosting the catalytic performance[127-129].

Voiry *et al.* reported a highly strained WS_2 nanosheet with abundant metallic 1T phase as an efficient catalyst for hydrogen evolution [Figure 10A][130]. Compressive and tensile strain was both produced in the highlighted zigzag chain superlattice region. Considering the transition from highly strained and distorted 1T phase to stable 2H phase at high temperatures, the monolayered WS_2 nanosheets were incrementally annealed to obtain samples with varying 1T phase content. As a consequence, higher temperatures led to a decreased concentration of 1T phase, resulting in a suppressed electrocatalytic activity [Figure 10B]. DFT calculations revealed that the adsorption of atomic hydrogen on the surface of distorted 1T phase was significantly influenced by strain, and proper tensile strain (2.7%) could lead to a near thermoneutral free energy for a maximized electrocatalytic activity [Figure 10C]. Similarly, Hwang *et al.* reported the combinations of 2H/1T phase transition and bending strain by rolling up MoS_2 nanosheets; the self-induced uniaxial strain caused by rolling-up allowed the lamellar sliding and high catalytic activity for hydrogen evolution reactions (HER)[131].

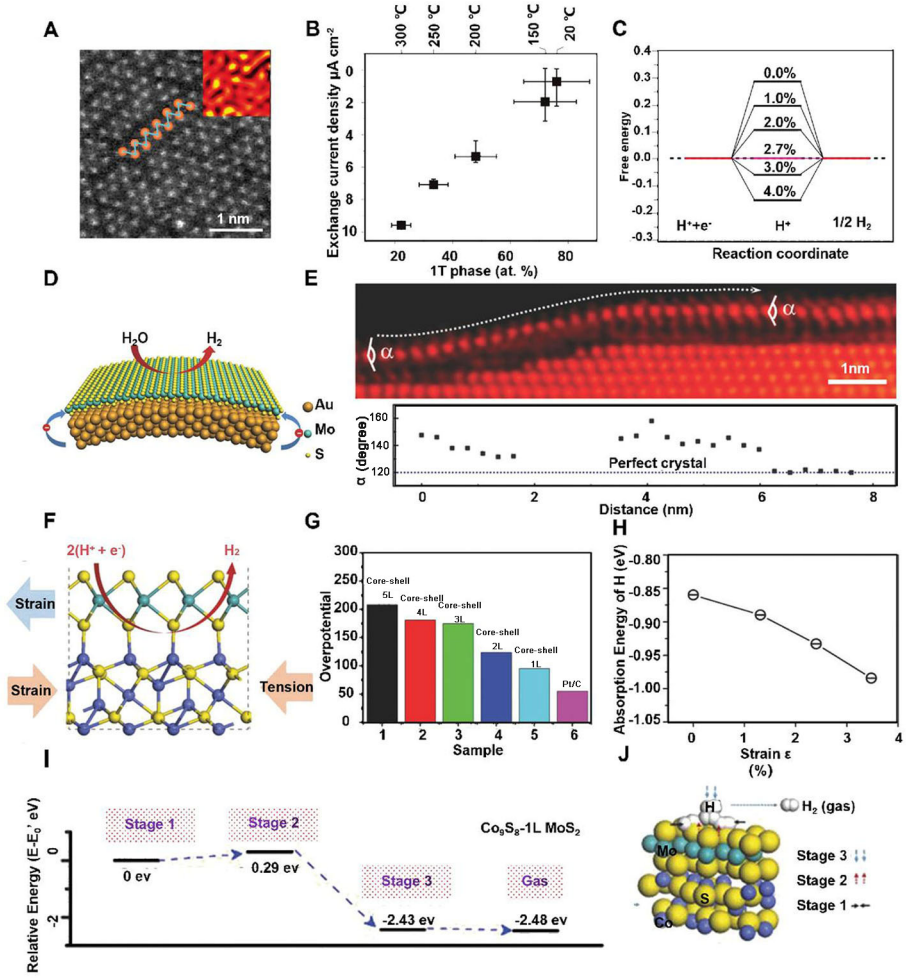

Figure 10. Strain engineering on electrocatalysis and its mechanism analysis. (A) High-resolution STEM image of a WS_2 monolayer exhibiting the highly distorted and strained 1T phase; (B) Relationship between 1T phase concentration and catalytic activity at different temperatures; (C) The absorption free energy of atomic hydrogen on the surface of distorted 1T phase under different strains; (A-C): quoted with permission from Voiry *et al.*[130]; (D) Schematic illustration of HER catalyzed by a monolayer MoS_2 on nanoporous gold; (E) Annular bright-field STEM image illustrating the variation in S-Mo-S bonding angles (α); (D-E): quoted with permission from Tan *et al.*[132]; (F) Schematic diagram of a core/shell nanostructure consisting of Co_9S_8 and single-layer MoS_2; (G) Comparison of overpotentials for HER at 10 mA·cm^{-2} among various Co_9S_8/nL MoS_2 (n = 1-5) and Pt/C catalysts; (H) Absorption energy of H in strained MoS_2 with ε% strain; (I) Reactive pathways for the transformation of hydrogen atoms into hydrogen molecules on Co_9S_8/1L MoS_2 for HER; (J) Schematic of hydrogen atom transforms to hydrogen molecule on the surface of Co_9S_8/1L MoS_2; (F-J): quoted with permission from Zhu *et al.*[134]. HER: Hydrogen evolution reactions; STEM: scanning transmission electron microscopy.

In addition to the strain introduced via phase transition, strain can also be introduced by the external substrate to optimize the electrocatalytic properties of materials. Tan *et al.* fabricated a strained monolayer MoS_2 with controllable out-of-plane strain for higher HER catalytic activity[132]. A 3D nanoporous gold (NPG) substrate with a curved internal surface was employed for the growth of a continuous monolayer of MoS_2 [Figure 10D], which provided a source of strain and served as a conductive channel for fast charge transfer and transport. The annular bright-field STEM image revealed a significant distortion of the S-Mo-S lattice, which was attributed to the strong coupling between the MoS_2 layer and the curved gold surface [Figure 10E]. As a result, the as-fabricated monolayer MoS_2 showed the best HER performance due to the out-of-plane strain introduced by lattice bending. Subsequently, Lee *et al.* employed contact printing to transfer vacuum-filtered MoS_2 nanosheets onto an Ag/PET substrate, which functioned as the working

electrode for HER[133]. By mechanical bending of the PET substrate, up to 0.02% tensile strain could be introduced into the MoS_2 thin film. With the increase of tensile strain, the strained MoS_2 nanosheets showed a lower Tafel slope and a steeper polarization curve than strain-free MoS_2 nanosheets, demonstrating the correlation between mechanically bending strain and electrochemical activities.

In another work, a precise surface strain tuning strategy was proposed for Co_9S_8/MoS_2 core/shell nanocrystals via lattice mismatch[134]. With the MoS_2 layers changing from 1 to 5, a continuous adjustment of the bond lengths of Co-S and Mo-S occurred at the interface of Co_9S_8 and MoS_2, resulting in tensile strain on the MoS_2 shell and compressive strain on the Co_9S_8 core [Figure 10F]. As a result, the strained Co_9S_8/1L MoS_2 (3.5%) manifested the best HER performance [Figure 10G]. Reaction pathways and absorption energy of hydrogen atoms for the strained MoS_2 were investigated to elucidate the correlation between lattice strain and HER performance [Figure 10H]. The hydrogen absorption (stage 1 to stage 2) is the rate-determining step of the reaction. As a result, the larger strain in MoS_2 made a more negative $\triangle E_H$ (from -0.85 to -0.98 eV) [Figure 10I], indicating an enhanced combination of hydrogen atoms on a strained MoS_2 surface and a better HER performance. Further, electron density maps revealed that the strain at the Co-S-Mo interface led to a redistribution of electron density, resulting in a low energy barrier for the reaction [Figure 10J].

CONCLUSION AND OUTLOOK

Strain engineering is a crucial approach for modulating the electronic structure and properties, which have garnered significant attention in 2D materials. This article first provides an overview of the fundamental understanding of the strain. Then, several methods for introducing strain into 2D materials are proposed. Lastly, the application of strain engineering in energy storage, electrocatalysis, and photocatalysis are reviewed. Due to the unique morphology of 2D materials (high Young's modulus and large surface area), they exhibit exceptional resistance to surface strain without fracturing. Additionally, the confinement of electrons within a 2D plane renders them highly susceptible to strain. As predicted, even minor strain can induce change in the lattice structure, thereby dramatically tuning its physical properties. Such a unique advantage endows 2D materials with more possibilities in the fields of energy storage and conversion. Despite the rapid development and advances of strain engineering for 2D materials, there are still some problems to be solved.

Decoupling strain effect

In 2D materials, the relationship between defects and strain is always entangled and indistinguishable. In other words, defects will be generated to relax the strain near the distorted region, while inherent defects of the material introduce strain. It still needs more rational experimental design and theoretical models for decoupling the effects of strain. Such complex synergy of strain and other factors requires complementary experimental and theoretical studies to deeply understand their interactions. These synergistic effects present novel opportunities for expanding the properties and applications of 2D materials.

Effective characterization techniques

A comprehensive comprehension of surface strain effects necessitates advanced characterization methods for both *in-situ* and *ex-situ*, which requires more advanced characterization techniques. There are numerous physiochemical characterizations of strain for 2D materials, such as Raman and PL spectroscopy, X-ray absorption spectroscopy, atomic-resolution electron microscopy, *etc*. However, these methods are mainly limited to low spatial resolution. It is still urgent for advanced strain characterization techniques to have a definite description.

Theoretical framework

Although DFT calculations, molecular dynamics, and continuum mechanics simulations have been widely used to explain the role of strain in energy storage and conversion, there is still a lack of sufficient theoretical guidance to rationally design a material with better performance. The d-band theory revealed the relationship between strain and catalytic properties for the first time, but it seems that it cannot fully explain the relationship between the strain-induced change in adsorption and reactions. Meanwhile, the relationship between strain and energy storage is mostly confined to theoretical calculations, with few proposed theories regarding strain-directed energy storage. The establishment of more rational theoretical frameworks is necessary to elucidate the fundamental intrinsic relationship between strain engineering and material properties.

In general, strain engineering of 2D materials provides an effective approach to modulating their physicochemical properties and expanding their applications in the realm of energy storage and conversion. It is believed that through continuous exploration, the realm of strain engineering in 2D materials will gain a deeper understanding and broader prospects.

DECLARATIONS

Authors' contributions

Prepared the manuscript: Peng X, Chen L, Liu Y, Liu C, Huang H, Fan J
Performed manuscript editing: Xiong P, Zhu J

Availability of data and materials

Not applicable.

Financial support and sponsorship

This work was supported by the Natural Science Foundation of China (No. 22179062, 52125202, and U2004209), the Natural Science Foundation of Jiangsu Province (BK20230035), the Fundamental Research Funds for the Central Universities (No. 30922010303), and the Intergovernmental Cooperation Projects in the National Key Research and Development Plan of the Ministry of Science and Technology of PRC (No. 2022YFE0196800).

Conflicts of interest

All authors declared that there are no conflicts of interest.

Ethical approval and consent to participate

Not applicable.

Consent for publication

Not applicable.

Copyright

© The Author(s) 2023.

REFERENCES

1. Novoselov KS, Geim AK, Morozov SV, et al. Electric field effect in atomically thin carbon films. *Science* 2004;306:666-9. DOI
2. Plechinger G, Castellanos-gomez A, Buscema M, et al. Control of biaxial strain in single-layer molybdenite using local thermal expansion of the substrate. *2D Mater* 2015;2:015006. DOI
3. Wang L, Nilsson ZN, Tahir M, Chen H, Sambur JB. Influence of the substrate on the optical and photo-electrochemical properties of monolayer MoS_2. *ACS Appl Mater Interfaces* 2020;12:15034-42. DOI PubMed

4. Jiang S, Xie H, Shan J, Mak KF. Exchange magnetostriction in two-dimensional antiferromagnets. *Nat Mater* 2020;19:1295-9. DOI PubMed
5. Radisavljevic B, Radenovic A, Brivio J, Giacometti V, Kis A. Single-layer MoS_2 transistors. *Nat Nanotechnol* 2011;6:147-50. DOI PubMed
6. Yu H, Sun Q, Zhang T, Zhang X, Shen Y, Wang M. Is the strain responsible to instability of inorganic perovskites and their photovoltaic devices? *Mater Today Energy* 2021;19:100601. DOI
7. Chen W, Zhang R, Sun Y, Wang J, Fan Y, Liu B. Preparation, properties, and electronic applications of 2D Bi_2O_2Se. *Adv Powder Mater* 2023;2:100080. DOI
8. Yin Y, Kang X, Han B. Two-dimensional materials: synthesis and applications in the electro-reduction of carbon dioxide. *Chem Synth* 2022;2:19. DOI
9. Chen L, Lin X, Dang W, Huang H, Liu G, Yang Z. Tantalum oxide nanosheets/polypropylene composite separator constructing lithium-ion channels for stable lithium metal batteries. *Adv Compos Hybrid Mater* 2023;6:12. DOI
10. Liu C, Ye C, Wu Y, et al. Atomic-scale engineering of cation vacancies in two-dimensional unilamellar metal oxide nanosheets for electricity generation from water evaporation. *Nano Energy* 2023;110:108348. DOI
11. Phalswal P, Khanna PK, Rubahn HG, Mishra YK. Nanostructured molybdenum dichalcogenides: a review. *Mater Adv* 2022;3:5672-97. DOI
12. Zhang K, Feng S, Wang J, et al. Manganese doping of monolayer MoS_2: the substrate is critical. *Nano Lett* 2015;15:6586-91. DOI PubMed
13. Jin Y, Zeng Z, Xu Z, et al. Synthesis and transport properties of degenerate P-type Nb-doped WS_2 monolayers. *Chem Mater* 2019;31:3534-41. DOI
14. Li H, Du M, Mleczko MJ, et al. Kinetic study of hydrogen evolution reaction over strained MoS_2 with sulfur vacancies using scanning electrochemical microscopy. *J Am Chem Soc* 2016;138:5123-9. DOI
15. Liu C, Liu Y, Ma R, et al. Atomic cation-vacancy engineering of two-dimensional nanosheets for energy-related applications. *Mater Chem Front* 2023;7:1004-24. DOI
16. Shao G, Lu Y, Hong J, et al. Seamlessly splicing metallic $SnxMo_{1-x}S_2$ at MoS_2 edge for enhanced photoelectrocatalytic performance in microreactor. *Adv Sci* 2020;7:2002172. DOI PubMed PMC
17. Yang S, Liu F, Wu C, Yang S. Tuning surface properties of low dimensional materials via strain engineering. *Small* 2016;12:4028-47. DOI PubMed
18. Zheng SW, Wang HY, Wang L, Luo Y, Gao BR, Sun HB. Observation of robust charge transfer under strain engineering in two-dimensional MoS_2-WSe_2 heterostructures. *Nanoscale* 2021;13:14081-8. DOI PubMed
19. Miao Y, Zhao Y, Zhang S, Shi R, Zhang T. Strain engineering: a boosting strategy for photocatalysis. *Adv Mater* 2022;34:2200868. DOI
20. Shaikh JS, Shaikh NS, Sabale S, et al. A phosphorus integrated strategy for supercapacitor: 2D black phosphorus-doped and phosphorus-doped materials. *Mater Today Chem* 2021;21:100480. DOI
21. Yan Y, Ding S, Wu X, et al. Tuning the physical properties of ultrathin transition-metal dichalcogenides *via* strain engineering. *RSC Adv* 2020;10:39455-67. DOI PubMed PMC
22. Li H, Liu H, Zhou L, et al. Strain-tuning atomic substitution in two-dimensional atomic crystals. *ACS Nano* 2018;12:4853-60. DOI PubMed
23. Bonavolontà C, Aramo C, Valentino M, et al. Graphene-polymer coating for the realization of strain sensors. *Beilstein J Nanotechnol* 2017;8:21-7. DOI PubMed PMC
24. Chaste J, Missaoui A, Huang S, et al. Intrinsic properties of suspended MoS_2 on SiO_2/Si pillar arrays for nanomechanics and optics. *ACS Nano* 2018;12:3235-42. DOI PubMed
25. Wu Y, Wang L, Li H, Dong Q, Liu S. Strain of 2D materials *via* substrate engineering. *Chin Chem Lett* 2022;33:153-62. DOI
26. Akinwande D, Brennan CJ, Bunch JS, et al. A review on mechanics and mechanical properties of 2D materials - Graphene and beyond. *Extreme Mech Lett* 2017;13:42-77. DOI
27. Yang S, Chen Y, Jiang C. Strain engineering of two-dimensional materials: methods, properties, and applications. *InfoMat* 2021;3:397-420. DOI
28. Hammer B, Nørskov JK. Theoretical surface science and catalysis - calculations and concepts. *Adv Catal* 2000;45:71-129. DOI
29. Deng S, Sumant AV, Berry V. Strain engineering in two-dimensional nanomaterials beyond graphene. *Nano Today* 2018;22:14-35. DOI
30. Zhou K, Dai K, Liu C, Shen C. Flexible conductive polymer composites for smart wearable strain sensors. *SmartMat* 2020;1:e1010. DOI
31. Zhang H, Tersoff J, Xu S, et al. Approaching the ideal elastic strain limit in silicon nanowires. *Sci Adv* 2016;2:e1501382. DOI PubMed PMC
32. Mohiuddin TMG, Lombardo A, Nair RR, et al. Uniaxial strain in graphene by Raman spectroscopy: *G* peak splitting, Grüneisen parameters, and sample orientation. *Phys Rev B* 2009;79:205433. DOI
33. Lu J, Gomes LC, Nunes RW, Castro Neto AH, Loh KP. Lattice relaxation at the interface of two-dimensional crystals: graphene and hexagonal boron-nitride. *Nano Lett* 2014;14:5133-9. DOI PubMed
34. Li H, Contryman AW, Qian X, et al. Optoelectronic crystal of artificial atoms in strain-textured molybdenum disulphide. *Nat*

Commun 2015;6:7381. DOI PubMed PMC
35. Azcatl A, Qin X, Prakash A, et al. Covalent nitrogen doping and compressive strain in MoS_2 by remote N_2 plasma exposure. *Nano Lett* 2016;16:5437-43. DOI PubMed
36. Pierucci D, Henck H, Ben Aziza Z, et al. Tunable doping in hydrogenated single layered molybdenum disulfide. *ACS Nano* 2017;11:1755-61. DOI
37. Hsu WT, Lu LS, Wang D, et al. Evidence of indirect gap in monolayer WSe_2. *Nat Commun* 2017;8:929. DOI PubMed PMC
38. Yang J, Wang Y, Lagos MJ, et al. Single atomic vacancy catalysis. *ACS Nano* 2019;13:9958-64. DOI
39. Li Z, Lv Y, Ren L, et al. Efficient strain modulation of 2D materials via polymer encapsulation. *Nat Commun* 2020;11:1151. DOI PubMed PMC
40. Lee CH, Khan A, Luo D, et al. Deep learning enabled strain mapping of single-atom defects in two-dimensional transition metal dichalcogenides with sub-picometer precision. *Nano Lett* 2020;20:3369-77. DOI
41. Li L, Schultz JF, Mahapatra S, et al. Angstrom-scale spectroscopic visualization of interfacial interactions in an organic/borophene vertical heterostructure. *J Am Chem Soc* 2021;143:15624-34. DOI
42. Wu G, Han X, Cai J, et al. In-plane strain engineering in ultrathin noble metal nanosheets boosts the intrinsic electrocatalytic hydrogen evolution activity. *Nat Commun* 2022;13:4200. DOI PubMed PMC
43. Cao X, Huang A, Liang C, et al. Engineering lattice disorder on a photocatalyst: photochromic BiOBr nanosheets enhance activation of aromatic C-H bonds via water oxidation. *J Am Chem Soc* 2022;144:3386-97. DOI PubMed
44. Bhatt MD, Lee JS. Effect of lattice strain on nanomaterials in energy applications: a perspective on experiment and theory. *Int J Hydrog Energy* 2017;42:16064-107. DOI
45. Sharma SK, Sharma G, Gaur A, et al. Progress in electrode and electrolyte materials: path to all-solid-state Li-ion batteries. *Energy Adv* 2022;1:457-510. DOI
46. Xu X, Liang T, Kong D, Wang B, Zhi L. Strain engineering of two-dimensional materials for advanced electrocatalysts. *Mater Today Nano* 2021;14:100111. DOI
47. Khorshidi A, Violet J, Hashemi J, Peterson AA. How strain can break the scaling relations of catalysis. *Nat Catal* 2018;1:263-8. DOI
48. Deeksha, Kour P, Ahmed I, et al. Transition metal-basedcsts for oxygen evolution reaction. *ChemCatChem* 2023;15:e202300040. DOI
49. Dalrymple OK, Stefanakos E, Trotz MA, Goswami DY. A review of the mechanisms and modeling of photocatalytic disinfection. *Appl Catal B Environ* 2010;98:27-38. DOI
50. Jiang J, Pendse S, Zhang L, Shi J. Strain related new sciences and devices in low-dimensional binary oxides. *Nano Energy* 2022;104:107917. DOI
51. Xu Y, von Delius M. The supramolecular chemistry of strained carbon nanohoops. *Angew Chem Int Ed Engl* 2020;59:559-73. DOI PubMed
52. Lloyd D, Liu X, Christopher JW, et al. Band gap engineering with ultralarge biaxial strains in suspended monolayer MoS_2. *Nano Lett* 2016;16:5836-41. DOI
53. Liu B, Liao Q, Zhang X, et al. Strain-engineered van der waals interfaces of mixed-dimensional heterostructure arrays. *ACS Nano* 2019;13:9057-66. DOI
54. Conley HJ, Wang B, Ziegler JI, Haglund RF Jr, Pantelides ST, Bolotin KI. Bandgap engineering of strained monolayer and bilayer MoS_2. *Nano Lett* 2013;13:3626-30. DOI PubMed
55. Di J, Song P, Zhu C, et al. Strain-engineering of $Bi_{12}O_{17}Br_2$ nanotubes for boosting photocatalytic CO_2 reduction. *ACS Mater Lett* 2020;2:1025-32. DOI
56. Feng H, Xu Z, Wang L, et al. Modulation of photocatalytic properties by strain in 2D BiOBr nanosheets. *ACS Appl Mater Interfaces* 2015;7:27592-6. DOI
57. Franchini IR, Bertoni G, Falqui A, Giannini C, Wang LW, Manna L. Colloidal PbTe-aunanocrystal heterostructures. *J Mater Chem* 2010;20:1357-66. DOI
58. Zhang P, Cheng N, Li M, et al. Transition-metal substitution-induced lattice strain and electrical polarity reversal in monolayer WS_2. *ACS Appl Mater Interfaces* 2020;12:18650-9. DOI PubMed
59. Castellanos-Gomez A, Roldán R, Cappelluti E, et al. Local strain engineering in atomically thin MoS_2. *Nano Lett* 2013;13:5361-6. DOI PubMed
60. Ni W, Wang T, Schouwink PA, Chuang YC, Chen HM, Hu X. Efficient hydrogen oxidation catalyzed by strain-engineered nickel nanoparticles. *Angew Chem Int Ed Engl* 2020;59:10797-801. DOI PubMed
61. Chattot R, Le Bacq O, Beermann V, et al. Surface distortion as a unifying concept and descriptor in oxygen reduction reaction electrocatalysis. *Nat Mater* 2018;17:827-33. DOI PubMed PMC
62. Liu Y, Zeng C, Zhong J, Ding J, Wang ZM, Liu Z. Spintronics in two-dimensional materials. *Nanomicro Lett* 2020;12:93. DOI PubMed PMC
63. Bai S, Zhang N, Gao C, Xiong Y. Defect engineering in photocatalytic materials. *Nano Energy* 2018;53:296-336. DOI
64. Wang S, Wang L, Xie L, et al. Dislocation-strained MoS_2 nanosheets for high-efficiency hydrogen evolution reaction. *Nano Res* 2022;15:4996-5003. DOI
65. Mao Q, Deng K, Wang W, et al. N-doping induced lattice-strained porous PdIr bimetallene for pH-universal hydrogen evolution electrocatalysis. *J Mater Chem A* 2022;10:8364-70. DOI

66. Zhu Y, Yang H, Sun F, Wang X. Controllable Growth of Ultrathin P-doped ZnO Nanosheets. *Nanoscale Res Lett* 2016;11:175. DOI PubMed PMC
67. Liang S, Han B, Ou X, et al. Lattice-strained nickel hydroxide nanosheets for the boosted diluted CO_2 photoreduction. *Environ Sci Nano* 2021;8:2360-71. DOI
68. Zhao Y, Zhao Y, Waterhouse GIN, et al. Photocatalysts: layered-double-hydroxide nanosheets as efficient visible-light-driven photocatalysts for dinitrogen fixation (Adv. Mater. 42/2017). *Adv Mater* 2017;29:1703828. DOI
69. Zhang W, Cai L, Cao S, et al. Electrode materials: interfacial lattice-strain-driven generation of oxygen vacancies in an aerobic-annealed TiO_2(B) electrode (Adv. Mater. 52/2019). *Adv Mater* 2019;31:1930367. DOI
70. Choi SY, Kim SD, Choi M, et al. Assessment of strain-generated oxygen vacancies using $SrTiO_3$ bicrystals. *Nano Lett* 2015;15:4129-34. DOI PubMed
71. Li H, Tsai C, Koh AL, et al. Correction: corrigendum: activating and optimizing MoS_2 basal planes for hydrogen evolution through the formation of strained sulphur vacancies. *Nat Mater* 2016;15:364. DOI PubMed
72. Zhao Y, Zhao Y, Shi R, et al. Tuning oxygen vacancies in ultrathin TiO_2 Nanosheets to boost photocatalytic nitrogen fixation up to 700 nm. *Adv Mater* 2019;31:1806482. DOI PubMed
73. Jeong HY, Jin Y, Yun SJ, et al. Heterogeneous defect domains in single-crystalline hexagonal WS_2. *Adv Mater* 2017;29:1605043. DOI PubMed
74. Luo M, Guo S. Strain-controlled electrocatalysis on multimetallic nanomaterials. *Nat Rev Mater* 2017;2:17059. DOI
75. Lemme MC, Akinwande D, Huyghebaert C, Stampfer C. 2D materials for future heterogeneous electronics. *Nat Commun* 2022;13:1392. DOI PubMed PMC
76. Li MY, Shi Y, Cheng CC, et al. Epitaxial growth of a monolayer WSe_2-MoS_2 lateral p-n junction with an atomically sharp interface. *Science* 2015;349:524-8. DOI PubMed
77. Xie S, Tu L, Han Y, et al. Coherent, atomically thin transition-metal dichalcogenide superlattices with engineered strain. *Science* 2018;359:1131-6. DOI
78. Zhu Z, Svensson J, Persson AR, Wallenberg R, Gromov AV, Wernersson LE. Compressively-strained GaSb nanowires with core-shell heterostructures. *Nano Res* 2020;13:2517-24. DOI
79. Zhang C, Li MY, Tersoff J, et al. Strain distributions and their influence on electronic structures of WSe_2-MoS_2 laterally strained heterojunctions. *Nat Nanotechnol* 2018;13:152-8. DOI
80. Xiong P, Zhang F, Zhang X, et al. Strain engineering of two-dimensional multilayered heterostructures for beyond-lithium-based rechargeable batteries. *Nat Commun* 2020;11:3297. DOI PubMed PMC
81. Zhang Z, Chen P, Duan X, Zang K, Luo J, Duan X. Robust epitaxial growth of two-dimensional heterostructures, multiheterostructures, and superlattices. *Science* 2017;357:788-92. DOI
82. He K, Poole C, Mak KF, Shan J. Experimental demonstration of continuous electronic structure tuning via strain in atomically thin MoS_2. *Nano Lett* 2013;13:2931-6. DOI PubMed
83. Ni ZH, Yu T, Lu YH, Wang YY, Feng YP, Shen ZX. Uniaxial strain on graphene: Raman spectroscopy study and band-gap opening. *ACS Nano* 2008;2:2301-5. DOI
84. Zhang Q, Chang Z, Xu G, et al. Strain relaxation of monolayer WS_2 on plastic substrate. *Adv Funct Mater* 2016;26:8707-14. DOI
85. Huang M, Yan H, Chen C, Song D, Heinz TF, Hone J. Phonon softening and crystallographic orientation of strained graphene studied by Raman spectroscopy. *Proc Natl Acad Sci U S A* 2009;106:7304-8. DOI PubMed PMC
86. Hui YY, Liu X, Jie W, et al. Exceptional tunability of band energy in a compressively strained trilayer MoS_2 sheet. *ACS Nano* 2013;7:7126-31. DOI PubMed
87. Zeng M, Liu J, Zhou L, et al. Bandgap tuning of two-dimensional materials by sphere diameter engineering. *Nat Mater* 2020;19:528-33. DOI
88. Zong Z, Chen CL, Dokmeci MR, Wan K. Direct measurement of graphene adhesion on silicon surface by intercalation of nanoparticles. *J Appl Phys* 2010;107:026104. DOI
89. Lee JK, Yamazaki S, Yun H, et al. Modification of electrical properties of graphene by substrate-induced nanomodulation. *Nano Lett* 2013;13:3494-500. DOI
90. Zhang Y, Heiranian M, Janicek B, et al. Strain modulation of graphene by nanoscale substrate curvatures: a molecular view. *Nano Lett* 2018;18:2098-104. DOI
91. Reserbat-Plantey A, Kalita D, Han Z, et al. Strain superlattices and macroscale suspension of graphene induced by corrugated substrates. *Nano Lett* 2014;14:5044-51. DOI
92. Lloyd D, Liu X, Boddeti N, et al. Adhesion, stiffness, and instability in atomically thin MoS_2 bubbles. *Nano Lett* 2017;17:5329-34. DOI PubMed
93. Tomori H, Kanda A, Goto H, et al. Introducing nonuniform strain to graphene using dielectric nanopillars. *Appl Phys Express* 2011;4:075102. DOI
94. Cai W, Wang J, He Y, et al. Strain-modulated photoelectric responses from a flexible α-In_2Se_3/3R MoS_2 heterojunction. *Nanomicro Lett* 2021;13:74. DOI PubMed PMC
95. Liu Z, Zhu T, Wang J, et al. Functionalized fiber-based strain sensors: pathway to next-generation wearable electronics. *Nanomicro Lett* 2022;14:61. DOI PubMed PMC
96. Zhang CY, Zhang C, Pan JL, et al. Surface strain-enhanced MoS_2 as a high-performance cathode catalyst for lithium-sulfur batteries.

eScience 2022;2:405-15. DOI

97. Liu Z, Liu C, Chen Z, et al. Recent advances in two-dimensional materials for hydrovoltaic energy technology. *Exploration* 2023;3:20220061. DOI PubMed PMC
98. Xiong P, Zhang F, Zhang X, et al. Atomic-scale regulation of anionic and cationic migration in alkali metal batteries. *Nat Commun* 2021;12:4184. DOI PubMed PMC
99. Xiong P, Wu Y, Liu Y, et al. Two-dimensional organic-inorganic superlattice-like heterostructures for energy storage applications. *Energy Environ Sci* 2020;13:4834-53. DOI
100. Jiang K, Xiong P, Ji J, et al. Two-dimensional molecular sheets of transition metal oxides toward wearable energy storage. *Acc Chem Res* 2020;53:2443-55. DOI
101. Dai Z, Liu L, Zhang Z. 2D materials: strain engineering of 2D materials: issues and opportunities at the interface (Adv. Mater. 45/2019). *Adv Mater* 2019;31:1970322. DOI
102. Ma Y, Jang KI, Wang L, et al. Design of strain-limiting substrate materials for stretchable and flexible electronics. *Adv Funct Mater* 2016;26:5345-51. DOI PubMed PMC
103. Li F, Shen T, Wang C, Zhang Y, Qi J, Zhang H. Recent advances in strain-induced piezoelectric and piezoresistive effect-engineered 2D semiconductors for adaptive electronics and optoelectronics. *Nanomicro Lett* 2020;12:106. DOI PubMed PMC
104. Xiong P, Ma R, Wang G, Sasaki T. Progress and perspective on two-dimensional unilamellar metal oxide nanosheets and tailored nanostructures from them for electrochemical energy storage. *Energy Storage Mater* 2019;19:281-98. DOI
105. Hao J, Zheng J, Ling F, et al. Strain-engineered two-dimensional MoS_2 as anode material for performance enhancement of Li/Na-ion batteries. *Sci Rep* 2018;8:2079. DOI PubMed PMC
106. Oakes L, Carter R, Hanken T, et al. Interface strain in vertically stacked two-dimensional heterostructured carbon-MoS_2 nanosheets controls electrochemical reactivity. *Nat Commun* 2016;7:11796. DOI PubMed PMC
107. Ma M, Zhang S, Wang L, et al. Harnessing the volume expansion of MoS_3 anode by structure engineering to achieve high performance beyond lithium-based rechargeable batteries. *Adv Mater* 2021;33:2106232. DOI PubMed
108. Liu Y, Ding C, Yan X, et al. Interface-strain-confined synthesis of amorphous TiO_2 mesoporous nanosheets with stable pseudocapacitive lithium storage. *Chem Eng J* 2021;420:129894. DOI
109. Liu MC, Zhang BM, Zhang YS, et al. Regulating interlayer spacing with pillar and strain structures in Ti_3C_2 MXene layers by molecular welding for superior alkali metal ion storage. *Mater Today Energy* 2021;22:100832. DOI
110. Chen S, Fu Z, Zhang H, et al. Surface electrochemical stability and strain-tunable lithium storage of highly flexible 2D transition metal carbides. *Adv Funct Mater* 2018;28:1804867. DOI
111. Duan H, Yan N, Yu R, et al. Ultrathin rhodium nanosheets. *Nat Commun* 2014;5:3093. DOI
112. Sun Y, Liu Q, Gao S, et al. Pits confined in ultrathin cerium(IV) oxide for studying catalytic centers in carbon monoxide oxidation. *Nat Commun* 2013;4:2899. DOI
113. Bahadoran A, Ramakrishna S, Masudy-panah S, et al. Rational construction of a 0D/1D S-scheme CeO_2/$CdWO_4$ heterojunction for photocatalytic CO_2 reduction and H_2 production. *Ind Eng Chem Res* 2022;61:10931-44. DOI
114. Bhawna, Kumar S, Sharma R, et al. Catalytic heterostructured materials for CO_2 mitigation and conversion into fuels: a renewable energy approach towards a sustainable environment. *Sustain Energy Fuels* 2023;7:4354-95. DOI
115. Liu G, Zhen C, Kang Y, Wang L, Cheng HM. Unique physicochemical properties of two-dimensional light absorbers facilitating photocatalysis. *Chem Soc Rev* 2018;47:6410-44. DOI
116. Biele R, Flores E, Ares JR, et al. Strain-induced band gap engineering in layered TiS_3. *Nano Res* 2018;11:225-32. DOI
117. Feng J, Qian X, Huang CW, Li J. Strain-engineered artificial atom as a broad-spectrum solar energy funnel. *Nature Photon* 2012;6:866-72. DOI
118. Pak S, Lee J, Lee YW, et al. Strain-mediated interlayer coupling effects on the excitonic behaviors in an epitaxially grown MoS_2/WS_2 van der Waals heterobilayer. *Nano Lett* 2017;17:5634-40. DOI PubMed PMC
119. Wang SL, Luo X, Zhou X, et al. Fabrication and properties of a free-standing two-dimensional titania. *J Am Chem Soc* 2017;139:15414-9. DOI
120. Tao J, Wang X, Xu M, Liu C, Ge J, Xing W. Non-noble metals as activity sites for ORR catalysts in proton exchange membrane fuel cells (PEMFCs). *Ind Chem Mater* 2023;1:388-409. DOI
121. Mirshokraee SA, Muhyuddin M, Orsilli J, et al. Mono-, bi- and tri-metallic platinum group metal-free electrocatalysts for hydrogen evolution reaction following a facile synthetic route. *Ind Chem Mater* 2023;1:343-59. DOI
122. Wang H, Wang L, Luo Q, et al. Two-dimensional manganese oxide on ceria for the catalytic partial oxidation of hydrocarbons. *Chem Synth* 2022;2:2. DOI
123. He Y, Kang Z, Li J, Li Y, Tian X. Recent progress of manganese dioxide based electrocatalysts for the oxygen evolution reaction. *Ind Chem Mater* 2023;1:312-31. DOI
124. Chang CC, Chen CC, Hung WH, Hsu IK, Pimenta MA, Cronin SB. Strain-induced D band observed in carbon nanotubes. *Nano Res* 2012;5:854-62. DOI
125. Qian X, Fu L, Li J. Topological crystalline insulator nanomembrane with strain-tunable band gap. *Nano Res* 2015;8:967-79. DOI
126. Qiu Y, Rao Y, Zheng Y, Hu H, Zhang W, Guo X. Activating ruthenium dioxide via compressive strain achieving efficient multifunctional electrocatalysis for Zn-air batteries and overall water splitting. *InfoMat* 2022;4:e12326. DOI
127. Zhao W, Kozlov SM, Höfert O, et al. Graphene on Ni(111): coexistence of different surface structures. *J Phys Chem Lett* 2011;2:759-

64. DOI

128. You B, Tang MT, Tsai C, Abild-Pedersen F, Zheng X, Li H. Enhancing electrocatalytic water splitting by strain engineering. *Adv Mater* 2019;31:1807001. DOI

129. Mao X, Qin Z, Ge S, Rong C, Zhang B, Xuan F. Strain engineering of electrocatalysts for hydrogen evolution reaction. *Mater Horiz* 2023;10:340-60. DOI

130. Voiry D, Yamaguchi H, Li J, et al. Enhanced catalytic activity in strained chemically exfoliated WS_2 nanosheets for hydrogen evolution. *Nat Mater* 2013;12:850-5. DOI PubMed

131. Hwang DY, Choi KH, Park JE, Suh DH. Highly efficient hydrogen evolution reaction by strain and phase engineering in composites of Pt and MoS_2 nano-scrolls. *Phys Chem Chem Phys* 2017;19:18356-65. DOI PubMed

132. Tan Y, Liu P, Chen L, et al. Monolayer MoS_2 films supported by 3D nanoporous metals for high-efficiency electrocatalytic hydrogen production. *Adv Mater* 2014;26:8023-8. DOI PubMed

133. Lee JH, Jang WS, Han SW, Baik HK. Efficient hydrogen evolution by mechanically strained MoS_2 nanosheets. *Langmuir* 2014;30:9866-73. DOI PubMed

134. Zhu H, Gao G, Du M, et al. Electrocatalytic nanomaterials: atomic-scale core/shell structure engineering induces precise tensile strain to boost hydrogen evolution catalysis (Adv. Mater. 26/2018). *Adv Mater* 2018;30:1870191. DOI